Performance Trends of a Large Air-Cooled Steam Condenser during Windy Conditions

by

Francois G. Louw

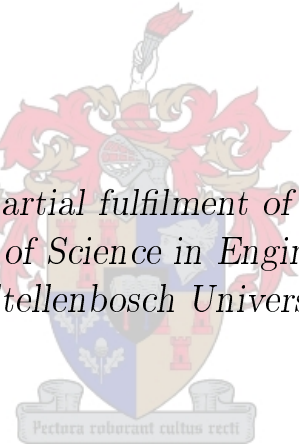

Thesis presented in partial fulfilment of the requirements for the degree of Master of Science in Engineering (Mechanical) at Stellenbosch University

Department of Mechanical and Mechatronic Engineering,
University of Stellenbosch,
Private Bag X1, Matieland 7602, South Africa.

Supervisor: Prof. D.G. Kröger

March 2011

Declaration

By submitting this thesis electronically, I declare that the entirety of the work contained therein is my own, original work, that I am the owner of the copyright thereof (unless to the extent explicitly otherwise stated) and that I have not previously in its entirety or in part submitted it for obtaining any qualification.

Date: .....

Abstract

Performance Trends of a Large Air-Cooled Steam Condenser during Windy Conditions

F.G. Louw

Department of Mechanical and Mechatronic Engineering,
University of Stellenbosch,
Private Bag X1, Matieland 7602, South Africa.

Thesis: MScEng (Mech)

March 2011

Large air-cooled steam condensers (ACSC's) find application in power stations and utilize arrays of large fans and heat-exchanger bundles to condense steam with a forced draft of ambient air. A numerical investigation was conducted in an attempt to extend knowledge on the flow distribution in the vicinity of a large ACSC (consisting of 384 fans) during windy periods. A three-dimensional numerical model of a large ACSC was subjected to various wind speeds in a cross and longitudinal direction (wind perpendicular and parallel to the longest side of the ACSC respectively). The study revealed that the flow approaching the ACSC could be classified as two- and three-dimensional depending on the inflow location of the ACSC. Fan performance is adversely affected due to separation at the upstream edge of the fan platform and is the worst in the two-dimensional flow area. Recirculation of hot plume was observed on the sides of the ACSC, parallel to the wind direction, as well as on the upstream periphery. Recirculation on the upstream edge increased in areas where the flow is two-dimensional. The study showed that a significant reduction in ACSC effectiveness occurs due to cross winds, whereas an overall effectiveness increase is seen for longitudinal winds. The effect of power station building placement on overall ACSC performance was also investigated. During windy conditions, fan performance mainly contributed to the reduction in ACSC performance, except for the cross-wind case where the wind blows from behind the boiler houses and turbine hall onto the ACSC. Wind mitigation measures in the form of different skirt and screen configurations were implemented on the Large ACSC, in an attempt to improve overall fan performance and reduce recirculation. The effect of individual skirts, screens and combinations of

these were investigated. Skirt widths provided an ACSC performance increase between 2-9%. A considerably greater improvement in ACSC performance, ranging from 8-30%, was achieved by means of screens. It is recommended that a further investigation be conducted to draw conclusions regarding the effect of various distances between the power station buildings and the ACSC on overall ACSC effectiveness. The orientation of the ACSC, regarding the dominant wind direction, should also be reconsidered in any future design.

Uittreksel

Tendense in die Verkoelingsvermoë van 'n Groot Lugverkoelde Stoom Kondensor gedurende Winderige Toestande

("Performance Trends of a Large Air-Cooled Steam Condenser during Windy Conditions")

F.G. Louw

Departement Meganiese en Megatroniese Ingenieurswese,
Universiteit van Stellenbosch,
Privaatsak X1, Matieland 7602, Suid Afrika.

Tesis: MScIng (Meg)

Maart 2011

Groot lugverkoelde stoom kondensors (LVSK's) word gebruik in kragstasies en bestaan uit rangskikkings van groot waaiers en vin-buis bundels om stoom te kondenseer deur middel van atmosferiese lug. 'n Numeriesie ondersoek was geloods in 'n poging om huidige kennis behelsende die vloeiverdeling in die nabyheid van 'n groot LVSK (wat bestaan uit 384 waaiers) te ondersoek gedurende winderige atmosferiese toestande. 'n Drie-dimensionele numeriese model van die groot LVSK was ondersoek deur die stelsel te belas met verskillende windsnelhede vanuit 'n *kruis* en *langs* rigting (wind loodreg en parallel aan die langste sy van die kondensor onderskeidelik). Die studie het twee- en drie-dimensionele vloei areas uitgewys, afhangend van die gebied waar die lug invloei. Waaiervermoë neem af as gevolg van wegbreking by die stroom-op rand van die LVSK en is die laagste vir die waaiers in die twee-dimensionele vloeigebied. Hersirkulasie van warm pluim lug was waargeneem by die kante, parallel aan die windrigting, asook rondom die stroom-op rand. 'n Toename in die stroom-op hersirkulasie was ook waargeneem namate die vloei twee-dimensioneel raak. Die effek van die kragstasiegeboue op die effektiwiteit van die LVSK was ook ondersoek. Die studie het gewys dat waaiervermoë die grootste bydrae maak tot die afname in die groot LVSK se effektiwiteit, behalwe in die geval waar die wind van agter die kragstasie geboue op die LVSK waai. In 'n poging om die afname in die LVSK se effektiwiteit teen te werk was verskillende loopvlakke en skerms op en rondom die LVSK aangebring. Die

effek van individuele loopvlakke, skerms asook 'n kombinasie van hierdie was ondersoek. Loopvlakke het oor die algemeen 'n verbetering tussen 2 en 9 % aangebring in die effektiwiteit van die LVSK, maar 'n groter verbetering was veroorsaak deur die implimentering van skerms wat in die orde van tussen 8 en 30 % was. Dit word voorgestel dat 'n verdere ondersoek geloods moet word om die effek van verskillende afstande tussen die gebou en die LVSK op die algemene effektiwiteit van die LVSK te bepaal. Die konvensionele oriëntasie van groot LVSK's moet ook heroorweeg word vir dominante windrigtings in die toekomstige ontwerp van groot LVSK's.

Acknowledgements

My acknowledgments go to the Lord, Jesus Christ, in whom I found salvation and is constantly teaching me truth, whether about life, people or engineering. I experience His smile throughout my life.

To professor Detlev G. Kröger who provided excellent guidance to this research. I will always remember the additional wisdom and laughter he added in the many meetings we had.

To my parents Irma and Johan, friends parents, many mentors, the multitude of friends surrounding me (whose names are too many) and my girlfriend Jeanne, for their aid through the tough times and their praise through the good times of this project. Each one of the mentioned is as close as family and the constant encouragement by them is/was appreciated incredibly.

To ESKOM for the funding and information applicable to this project.

To Qfinsoft and ANSYS for the provision of academic CFD software licenses and support.

To the staff of the Mechanical and Mechatronic Engineering Department, University of Stellenbosch and other departments of the university for all the administration, the provision of high performance computational facilities and constant help.

Dedications

To my family and friends

Contents

List of Figures

List of Tables

Nomenclature

Constants

$\pi =$ 3.141 592 654

Variables

A	Area	$[\,m^2\,]$
a	Variable	$[\ ]$
b	Variable	$[\ ]$
C	Inertial loss coefficient	$[\ ]$
c_p	Specific heat	$[\,J/kg \cdot K\,]$
d	Diameter	$[\,m\,]$
H	Height	$[\,m\,]$
h	Convection heat transfer coefficient	$[\,W/m^2 \cdot K\,]$
i	Variable	$[\ ]$
j	Variable	$[\ ]$
K	Loss coefficient	$[\ ]$
k	Thermal conductivity	$[\,W/m \cdot K\,]$
L	Length	$[\,m\,]$
m	Massflow	$[\,kg/s\,]$
N	Rotational speed	$[\,rev/min\,]$
Ny	Heat transfer parameter	$[\,1/m\,]$
n	Number	$[\ ]$
P	Power	$[\,W\,]$
p	Pressure	$[\,N/m^2\,]$
Q	Heat	$[\,W\,]$
q	Heat flux	$[\,W/m^2\,]$
Ry	Flow parameter	$[\,1/m\,]$
S	Source term	$[\ ]$
T	Temperature	$[\,K\,]$

UA	Overall heat transfer coefficient	$[\mathrm{W/m^2}]$
u	x-direction velocity	$[\mathrm{m/s}]$
V	Volume, Volumeflow	$[\mathrm{m^3}, \mathrm{m^3/s}]$
v	Velocity, y-direction velocity	$[\mathrm{m/s}]$
w	Work, z-direction velocity	$[\mathrm{W/m^2}, \mathrm{m/s}]$
x	Coordinate	$[\mathrm{m}]$

Greek symbols

$1/\alpha$	Viscous loss coefficient	$[\ ]$
β	Fan blade angle (measured at fan tip), Thermal expansion coefficient	$[^\circ, 1/\mathrm{K}]$
Γ	Diffusion coeffiecient	$[\ ]$
ε	Effectiveness	$[\ ]$
ζ	Fan blade angle (measured at fan hub)	$[^\circ]$
θ	Angle	$[^\circ]$
μ	Viscosity	$[\mathrm{kg/m \cdot s}]$
ρ	Density	$[\mathrm{kg/m^3}]$
σ	Ratio	$[\ ]$
Φ	Energy dissipation term	$[\ ]$
ϕ	Variable	$[\ ]$

Dimensionless groups

Pr	Prandtl number	$[\ ]$
Re	Reynolds number	$[\ ]$

Vectors and Tensors

$\mathbf{u}$	Velocity vector	$[\mathrm{m/s}]$

Subscripts

a	Air
b	Bundle, bellmouth, blade
c	Casing, contraction
cr	Chord
d	Dynamic

do	Downstream
E	Energy
e	Effective
F	Fan
Fs	Fan static
f	Fan-unit
fr	Frontal
h	Hub
he	Heat exchanger
i	Inner, inlet, number
id	Ideal
j	Jetting
M	Momentum
m	Mean
o	Outer, outlet
Q_F	Heat transfer per fan-unit
Q_U	Heat transfer per ACSC unit
r	Row
ref	Reference
s	Steam, supply, screen, static
ss	Static to static
t	Total, tube
ts	Tower support
up	Upstream
V	Volumetric
v	Vapor
vb	Velocity boundary
w	Wind, windwall, walkway(skirt)
x	Cartesian coordinate
y	Cartesian coordinate
z	Cartesian coordinate
θt	Inclined tube

Abbreviations

$ACSC$	Air-Cooled Steam Condenser
CFD	Computational Fluid Dynamics

UDF User Defined Function

Chapter 1

Introduction

1.1 Background

Thermodynamic cycles are used to harness energy from a heat source be it the sun, coal, nuclear or natural gas. In a thermodynamic cycle, work is done by continuously adding and extracting heat to and from a working fluid. The Rankine cycle, depicted in figure 1.1, has been widely adapted for use in the power generating industry where steam is utilized as an energy conveying medium.

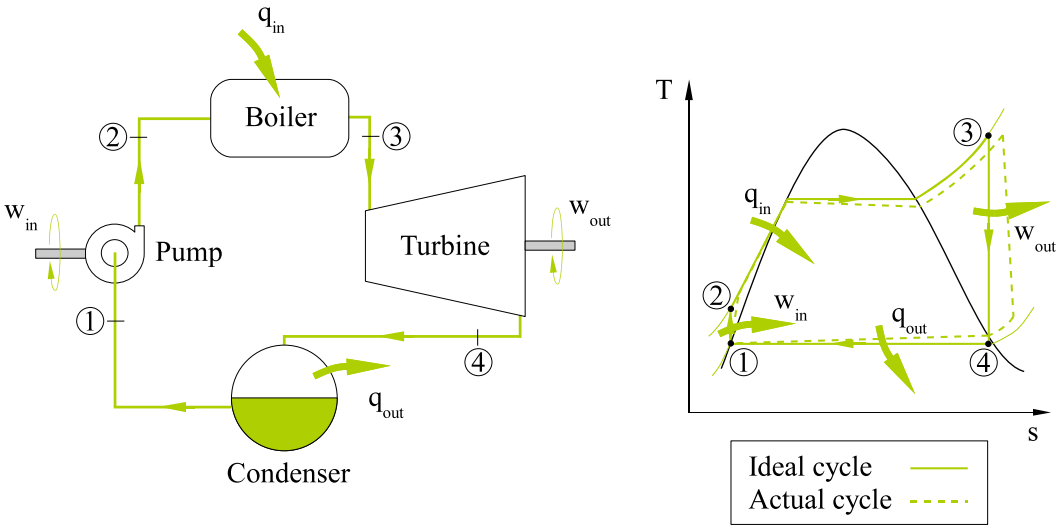

Figure 1.1: Rankine energy cycle (Adapted from Cengel and Boles (2006))

In a typical Rankine cycle, fluid is pumped to a boiler where heat is transferred to this fluid from a natural source e.g. coal. The fluid heats up and ultimately leaves the boiler as superheated vapor. After this, work is obtained

by allowing the vapor to expand in a turbine (or series of turbines). To complete the cycle, vapor exhausted from the turbine, is condensed in a condenser, rejecting unused heat.

Cengel and Boles (2006) mentions that steam is the most common working fluid used in vapor power cycles due to its multitude of desirable characteristics. Amongst these characteristics are its relatively low cost, availability and high enthalpy of vaporization. According to Kröger (2004) and Al-Waked and Behnia (2003) steam cycle power stations reject about 45 % of the initial heat input through a condenser, while approximately 15 % is rejected through the stack. It is therefore clear that dedicated attention be given to the design of effective cooling systems, since it plays an important part in the generating capacity of a power station.

Two main types of cooling exist, categorized as *wet-* and *dry-cooling*. *Wet-cooling* is the means of cooling with a fluid, which ordinarily is water. According to Bartz and Maulbetsch (1981), 75 % of coal-fired power plants built before 1970 used once-through cooling, relying on large water bodies such as oceans, dams or rivers, as energy sinks. An alternative to once-through cooling is found by means of wet-cooling towers depicted in figure 1.2 (a). Heated cooling water is sprayed onto a fill in the cooling tower which assists the process of evaporation. Evaporation is attained by means of a constant natural draft through the cooling tower. The water is cooled in this way and rains into a water basin from where it is returned to the condenser. Although this type of cooling provides a relatively high thermal efficiency (Tawney *et al.*, 2005), a problem emerges since fewer inland locations are able to support the massive water demand and strict environmental regulations complicates this cooling approach (Akhtar, 2000),(Swanekamp, 2002). Water consumed by these power stations for make-up water, cooling tower blowdown and ash scrubbing, is in the order of 2.5 l/kWh, which is a considerable amount compared to 0.2 l/kWh consumed by *dry-cooled* systems (Knirsch, July 1991). Due to the mentioned concerns regarding water, an increasing interest towards dry-cooling is noticed (EPRI, 2005).

Dry-cooling is an alternative to *wet-cooling* and finds increasing interest due to its water efficiency and practicality in arid areas. Cooling is provided by means of ambient air, removing heat from a thermal cycle through convection. Although various types of *dry-cooling* exist in steam cycle power stations, only forced draft air-cooled steam condensers (ACSC's) will be discussed, since the present research involves this cooling method.

A steam power generation cycle, with the utilization of ACSC's for cooling, is shown in figure 1.3. A typical ACSC, consists of a number of finned tube bundles arranged in an A-frame formation to reduce the total plant surface

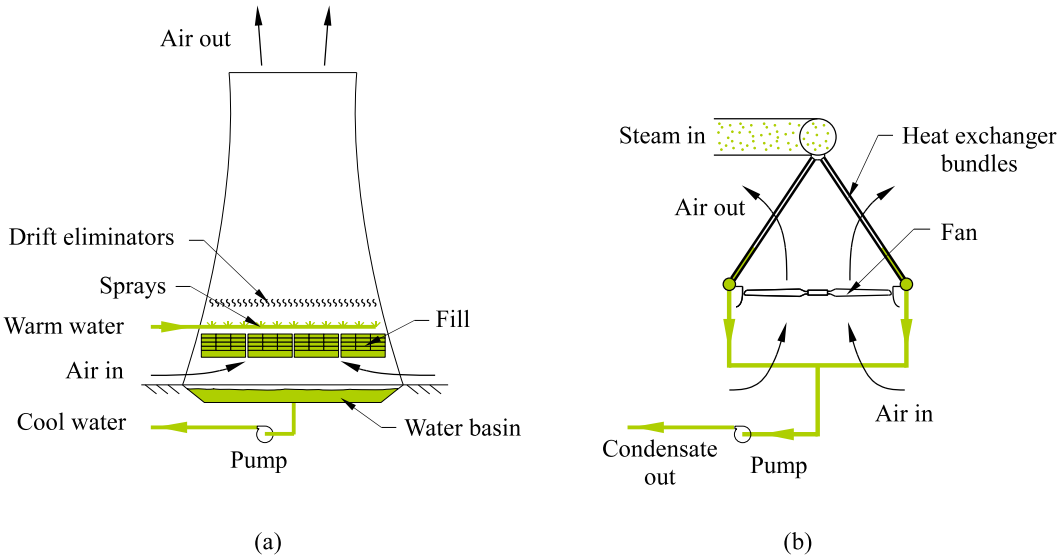

Figure 1.2: Schematic of (a) a wet-cooling tower and (b) an air-cooled condenser

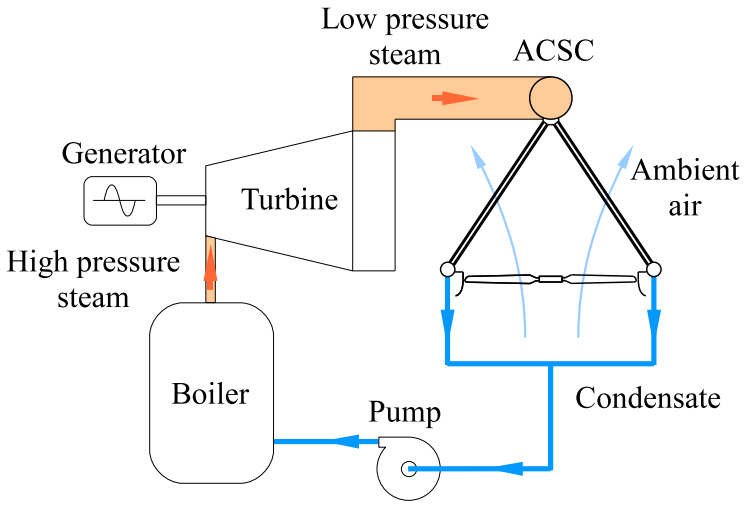

Figure 1.3: A typical steam cycle cooled by an ACSC

area and allows the effective drainage of condensate. Exhausted turbine steam flows through a header duct and is directly introduced into these finned tubes. Heat is transferred to the atmosphere by means of a forced draft, induced by a series of fans, situated beneath the finned tube bundles. The induced draft across the bundles causes steam to condense inside the tubes and to flow out into a condensate duct.

According to Larinoff *et al.* (1978) and Kröger (2004) air-cooled condensing found application in small power generating systems as early as the 1930's. Later on, a larger air-cooled condenser was constructed at the 365 MWe Wyo-

dak power station near Gilette in the USA, which consisted of 11 x 6 fans plus an extra prototype row of 6 fans. This plant came into operation in 1978 and held some challenges due to it's high altitude above sea level (1240 m) and extreme climatic temperatures of $-40\,^{\circ}\mathrm{C}$ to $43\,^{\circ}\mathrm{C}$. Knirsch (July 1991) and Kröger (2004) both report that it was the largest ACSC built at that time and held this status until the 6 x 665 MWe Matimba power station came into operation in 1991.

Due to the coal rich environment, South Africa's main electricy supplier (ESKOM), made the decision to construct the Matimba power station in Lephelale, South Africa. However, a local deficiency of water led to the construction of the current largest forced draft air-cooled power station in the world.

Matimba's ACSC consists of elliptic finned tube bundles arranged in an A-formation on top of 288 axial flow fans with a diameter of approximately 9 m and is situated at an elevation of 45 m above ground level. The entire ACSC covers a plan area of 32 300 m^2 and is placed against the turbine hall as can be seen in figure 1.4. This placement favors condenser performance during dominant Easterly winds, since air is obstructed by the turbine hall and forced upwards into the ACSC. However, Goldschagg (1993) reports that adverse ambient conditions such as strong winds, Westerly winds and extreme temperatures greatly affect the performance of the Matimba ACSC due to hot plume recirculation and poor fan performance as a consequence of distorted air inflow on the periphery of the ACSC.

Figure 1.4: 3990 MWe Matimba power station

Due to a mentioned global tendency toward dry-cooling, further investiga-

tion is required in order to optimize ACSC performance for the widest range of atmospheric conditions.

1.2 Literature survey

The literature survey of the present study follows in a chronological order and shows the development of forced draft air-cooled heat exchanger technology.

An article was released by **Monroe (1979)** on improving the overall effectiveness of air-cooled heat exchangers. It was noticed that among other problems in heat exchanger design specifications, a reduction in system performance also occurred due to hot plume recirculation (figure 1.5). This was especially noticed in forced draft air-coolers where low exit velocities are evident. It was also found that mechanical energy losses, due to flow separation at the fan inlets, reduce fan performance. It was recommended that the air velocity, approaching the heat exchanger, should not exceed half of the velocity through the fan throat. The article proposed that recirculation would be reduced by the implementation of baffles (windwalls) at the flow exit as well as to increase the exit flow velocity.

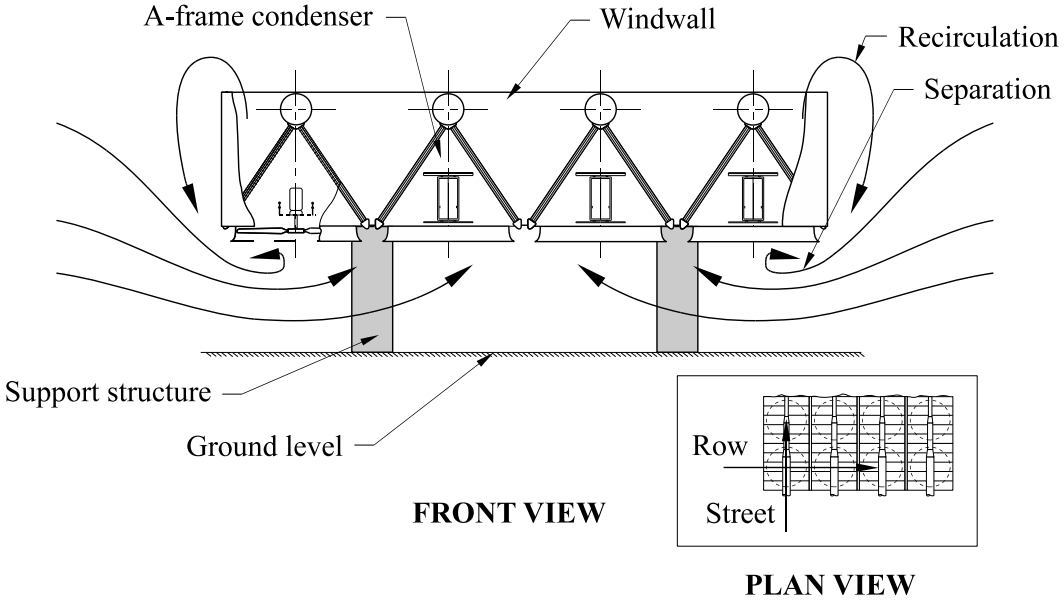

Figure 1.5: Schematic of plume recirculation and flow separation

Kröger (1989) analytically, numerically and experimentally investigated the reduction of performance in a mechanical draft heat exchanger due to recirculation. A two-dimensional model was considered for which an equation

is presented to calculate the approximate effectiveness of a generic heat exchanger. This equation was derived as a function of the flow, thermal and geometric characteristics of the heat exchanger excluding the influence of mixing and heat transfer in the air. Kröger (1989) concluded that experimentally predicted values followed a similar trend to the values obtained analytically, but were generally found to be higher. Mention was made that the accuracy of the experimental results could possibly have been affected by the size constraint of the test facility, used to model a scaled version of the heat exchanger. Numerical predictions included heat transfer and flow mixing, and these values were generally lower than values abtained by the other two methods.

Regarding mechanical energy losses through heat exchangers, **Van Aarde (1990)** conducted experiments on the air flow through a forced draft A-frame heat exchanger in which certain flow correlations and pressure loss coefficients were derived. It was concluded that flow through the heat exchanger is influenced by the semi-apex angle of the bundle arrangement, the loss coefficient through the bundle, the steam pipe diameter and the distance between separate A-frames. Notably atmospheric winds also had a significant effect on the performance of the heat exchanger.

Similar work to that of Kröger (1989) was done by **Conradie (1991)** who conducted a two-dimensional analytical and full scale experimental investigation (at Matimba power station, South Africa) into hot plume recirculation. Once again equations were derived to approximate performance evaluations of air-cooled heat exchangers subject to plume recirculation. The study reveals that the proper orientation and layout of a heat exchanger with respect to nearby structures, local topography and prevailing winds, will lead to a reduction in plume recirculation.

As mentioned in section 1.1, **Goldschagg (1993)** confirms plume recirculation occurring at the condenser of Matimba power station, South Africa, during adverse winds. The lack of sufficient cooling ultimately led to a detrimental increase in turbine back-pressure and sometimes turbine trips. Certain structural and other modifications were undertaken, which ultimately improved the condenser performance under these conditions.

Du Toit *et al.* (1993) studied the influence of the air flow pattern in the vicinity of a mechanical-draft heat exchanger subject to cross-wind. A two-dimensional model was solved by means of computational fluid dynamics (CFD), in which the effect of different platform heights and wind speeds on overall heat exchanger performance was investigated. It was concluded that recirculation has a significant effect on the performance of the heat exchanger and that heat transfer should be based on the local flow conditions as well as the influence of the flow field on the fans. It was recommended that a further

study should be done in three dimensions in order to obtain a better understanding of the problem.

The literature to this point offered many solutions to plume recirculation occurring at air-cooled heat exchangers, but no focus was placed on fan performance. A focus on the design and performance of axial flow fans for the use in forced draft air-cooled heat exchangers were yet unknown and thus some investigation into this field commenced.

Thiart and Von Backström (1993) developed an *actuator-disk* fan model which uses blade element theory to numerically predict the flow field in the vicinity of the fan blades without explicitly modeling the blade geometry. The model showed good correlation to experimental results for normal axisymetric flow into the fan, but deviated for cases of cross-flow beneath the fan inlet. It was also mentioned that this method was computationally expensive to use and further investigation was required to make this method viable for engineering purposes.

Bruneau (1994) designed a robust axial flow fan for cooling tower applications, solely to tolerate distorted inlet flows. The fan, based on the NASA LS aerofoil profile, was consequently named the *B-fan*. Fan tests were conducted according to British standard BS 848 (Type A) in order to validate the fan performance in comparison with other industrial fan types for similar applications. Results obtained for the *B-fan* indicated a higher design point static efficiency and static pressure rise compared to the other fans. However, Bruneau (1994) mentions that fan testing occurred under ideal circumstances. Further testing was needed to determine the fan performance under distorted inlet conditions.

Salta and Kröger (1995) conducted two-dimensional experiments to research the reduction in volume flow rate through a single street of fans in an air-cooled heat exchanger by varying the distance between ground level and the fan platform. The results led to the derivation of empirical correlations for heat exchanger volume flow rate as a function of platform height. An exponential increase in volume flow rate was noticed as the fan platform was raised. The addition of a skirt next to the periphery fan also significantly improved the volume flow rate through the edge fan, especially at low platform heights.

Duvenhage *et al.* (1995) conducted a numerical and experimental investigation to determine the effect of distorted inflow on fan performance in a forced draft air-cooled heat exchanger. Similar to Salta and Kröger (1995), Duvenhage *et al.* (1995) found that changes in fan platform height caused similar changes in volume flow through the fans. Three different fan inlet shrouds were also investigated i.e. Cylindrical, Conical and Bell type inlet. Since me-

chanical losses through the Bell type inlet was in the order of zero it proved to be superior in comparison with the other inlet types. It was concluded that the inlet shroud be carefully chosen when a forced-draft ACSC is being designed.

Work done by **Meyer and Kröger (2001*a*)** involved experiments on different types of finned-tube heat exchangers determining to what extent the air inflow angle across the heat exchanger influenced the pressure loss coefficient. Separation was noticed at the leading edge between two fins which increased as the air inlet angle increased. A correlation was derived for the heat exchanger pressure loss coefficient, concluding that it is mainly influenced by the tube cross-sectional area.

Stinnes and Von Backström (2002) experimentally tested air-cooled heat exchanger fans in a test tunnel, according to British standard BS 848 (Type A). These tests were done to determine the effect of off-axis inflow on fan performance up to an angle of 45 °. It was found that these different inflow angles had a negligible effect on fan power consumption as well as total-to-total static pressure rise. However, the effect of distorted air inflow, inlet bellmouths and skirts were beyond the scope of the research.

Additional work was done by **Meyer and Kröger (2003)** to determine to what extent fan performance characteristics influenced the plenum chamber aerodynamic behavior. Numerical simulation of the mentioned *B-fan* was done using the "actuator disk" model as presented by Meyer and Kröger (2001*b*). The numerical study revealed that aerodynamic behavior is highly effected by the type of fan, the mounted angle of the fan blades as well as the volume flow through the fan and thus the maximum kinetic energy recovery in the plenum does not necessarily coincide with the maximum fan static efficiency.

Meyer (2005) numerically investigated the effect of inlet flow distortions on fan performance in a multi-row air-cooled heat exchanger. In some instances comparison was found with the work of Duvenhage *et al.* (1995) and Salta and Kröger (1995). It was also confirmed that the first row of fans is affected the most, but that a skirt on the periphery of the fan platform improves flow into the axial fan by moving the point of flow separation away from the fan inlet shroud.

Bredell (2005, 2006) numerically investigated the performance of two different axial flow fans for the application in ACSC's by essentially modeling a two-dimensional street of fan units, situated in a typical section of an ACSC, using the "actuator disk" model. Once again it was shown that cross-flow beneath the fan platform resulted in separation and distortion of flow at fan inlets, which reduced the volumetric flow rate through the fans nearest to the ACSC upstream periphery. This flow rate was also dependent on the type of

fan. Mention is made that the addition of a solid (non-porous) skirt along the side and a porous screen beneath the ACSC significantly improves the air flow through the entire condenser and subsequently also the thermal effectiveness.

Gu *et al.* (2005) and **Gu *et al.* (2006)** experimentally analyzed the wind effects on a scale model of a large ACSC of a specific power plant in China using a wind tunnel. As with Matimba, the ACSC is situated next to the turbine hall and boiler houses. It was once again confirmed that plume recirculation could be minimized through an increase in windwall as well as ACSC platform height.

Hotchkiss *et al.* (2006) continued the research of Stinnes and Von Backström (2002) by numerically simulating the oblique flow of air into the fan, using the "actuator disk" fan model of Meyer and Kröger (2001*b*). The numerical solutions confirmed similar trends to the experimental results of Stinnes and Von Backström (2002), but slightly under- and over-predicted the fan power consumption and fan static efficiency respectively. The numerical model thus proved relatively accurate up to an angle of 45 °.

Van Rooyen (2007, 2008) investigated the performance of a general ACSC, consisting of 30 fan units, under windy conditions from different directions. Once again the "actuator disk" model was employed through CFD in order to model the fans in the condenser. Due to a limited amount of computational power, three-dimensional modeling of the entire ACSC was done by simulating some of the individual fans, whereafter a number of interpolation schemes were used to obtain values for the fans not modeled. Separation of flow at the ACSC periphery and hot plume recirculation was noticed and trend wise showed similarities with the work of Bredell (2005). Van Rooyen (2007) also confirmed the following:

- A marginal reduction in ACSC performance could be seen due to hot plume recirculation.
- The ACSC performance was adversely affected by the shortage of ambient air through some fan units on the ACSC periphery due to separation.
- Modifications such as skirts on the ACSC periphery and porous screens below the ACSC improved the overall performance under windy conditions.

Liu *et al.* (2009) numerically investigated the effect of wind on recirculation occurring at a power plant in China. The entire ACSC as well as surrounding buildings were modeled using CFD through which it was shown that adverse plume recirculation occurred during strong winds, especially if

the ACSC is situated downstream of the boiler houses. Overall ACSC performance was also enhanced by increasing periphery fan speed to force more ambient air through these fan units during windy conditions.

Similar research to Liu *et al.* (2009) was done by **Gao *et al.* (2009)** who numerically simulated the effect of wind on the performance of a similar ACSC. However Gao *et al.* (2009) focused on fan performance as well as plume recirculation. The obtained results showed that ACSC performance was the worst for the case where wind blew onto the ACSC from across the power station buildings where recirculation was the main contributor to the reduced ACSC performance.

The ACSC of Van Rooyen (2007), consisting of 30 fan units, was also numerically investigated by **Joubert (2010)** to determine and improve the overall performance of the ACSC by mainly improving the fan performance. Unlike Van Rooyen (2007), Joubert (2010) held a greater amount of computational power and solved the flow through all the fans in the ACSC simultaneously using the "pressure-jump" method for fan modeling. This method was preferred to avoid the computationally expensive "actuator disk" model and was justified by correlation to the work of Van Rooyen (2007) in most cases, with some exception in cases with high wind velocities. Many additions and modifications were made to the general ACSC to investigate the individual effects on fan performance such as ACSC height variation, bellmouth inlet alternatives, different fan types and the addition of a variety of skirts along the periphery of the ACSC and porous screens below the ACSC. Once again it was found that the addition of skirt along the periphery of the ACSC and the installation of a porous screen below the ACSC posed the most cost effective and practical solution. These modifications resulted in an increase of 11.3 % in ACSC performance compared to the poorest performance of the unmodified ACSC.

Owen (2010) developed a two-step numerical modeling approach to investigate the performance of an ACSC also evading the computationally expensive "actuator disk" fan model by using the "pressure-jump" method. The ACSC of El Dorado power station in Nevada, USA, consisting of 30 fan units, was numerically modeled to simulate wind effects on its overall performance. Numerical results were found to be in good agreement with measurements taken on site. Owen (2010) mentions that reduced fan performance evidently has a far more significant influence on ACSC performance than plume recirculation. The advantage of modifications such as a periphery skirt and porous screens below the ACSC was confirmed. It was found that increasing the fan power of the periphery fans under windy conditions has a limited benefit, but might be valuable if it is considered in the design phase of an ACSC.

A thorough understanding of the flow field and associated phenomena about a mechanical-draft heat exchanger is imperative for optimal design of such a system (Du Toit *et al.*, 1993). Literature ((Kröger, 1989), (Du Toit *et al.*, 1993), (Hotchkiss *et al.*, 2006), (Bredell, 2005), (Van Rooyen, 2007), (Liu *et al.*, 2009), (Owen, 2010) and (Joubert, 2010)) has shown that CFD simulation can effectively be implemented to obtain better knowledge of the flow field around such heat exchangers and ultimately provide valuable information to estimate heat exchanger performance.

1.3 Research objective

Efficiency is a main concern in any thermal cycle and consequently also in power stations. Efficient cooling in a power station promotes efficient electricity production. With the mentioned trend towards dry-cooling and the construction of large ACSC's such as Matimba, a need arises to investigate the performance of these large systems, especially under windy conditions, since a significant reduction in performance occurs under these circumstances. Owen (2010) mentions that experiments on such large systems can amount to significant costs. Thus a seemingly cheaper and easier alternative is the use of CFD simulation.

Previous research done by Bredell (2005), Van Rooyen (2007), Owen (2010) and Joubert (2010) simulated the effect of distorted fan inflow on overall ACSC performance. The work of Bredell (2005) and Van Rooyen (2007) provided valuable insight into the numerical simulation of fans and ACSC's. This created a foundation for the work of Owen (2010) and Joubert (2010) who successfully simulated the effect of wind on full scale ACSC's consisting of 30 fans.

The present research project attempts to further this research by investigating the wind effect on an ACSC similar (but not identical) to the ACSC of the 4800 MWe Medupi (Pretorius and Du Preez, 2009) steam cycle power plant shown in figure 1.6. The ACSC consists of 384 individual fan units and has an overall surface footprint of approximately 72300 m^2. The investigated ACSC will conveniently be referred to as the Large ACSC throughout the remainder of the present study.

It should be mentioned that, due to a limit in computational resources, some simplifications to the numerical condenser model were made in the present study. These simplifications and numerical procedures will be discussed in greater detail in chapter 3.

As a first attempt, the numerical modeling (done in commercial code, *Flu-*

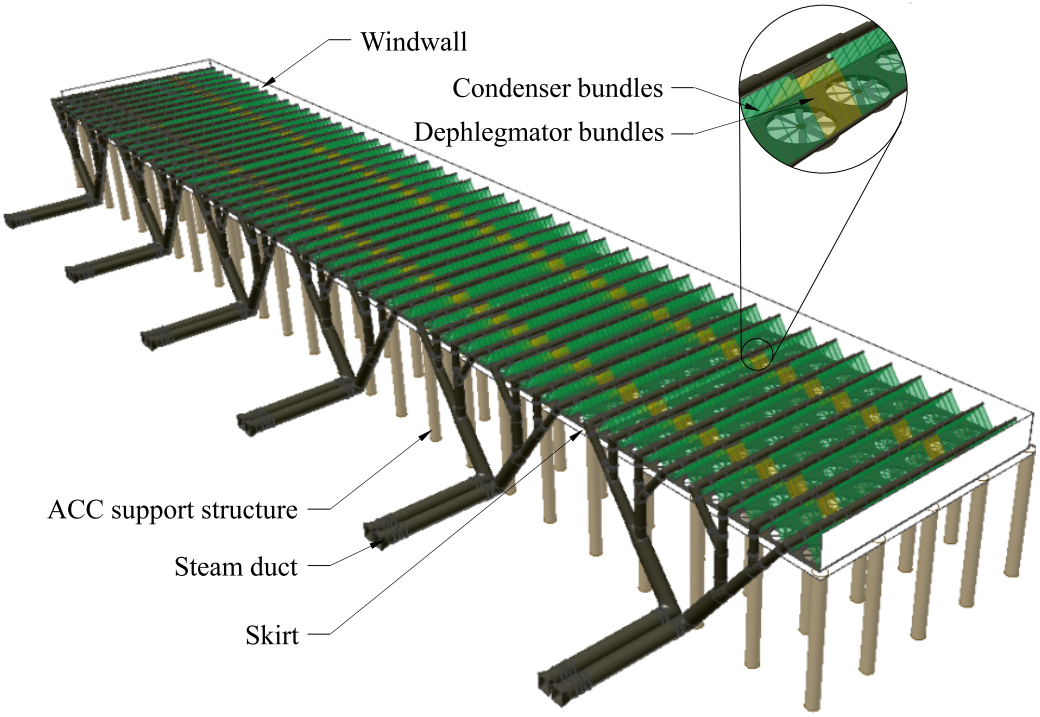

Figure 1.6: Schematic of the Medupi ACSC

ent 12) of the Van Rooyen (2007) ACSC system will be repeated to gain confidence in the numerical procedure used for the present research. Results obtained from this simulation will then be compared to results of Van Rooyen (2007), Owen (2010) and Joubert (2010) in order to confirm the validity of this numerical approach. Once the ACSC of Van Rooyen (2007) is successfully simulated the numerical modeling of the Large ACSC will commence in order to determine the effect of wind on the effectiveness the large ACSC.

The main objectives of the present study are set out as follow:

- Design of a simplified numerical ACSC models, without platform supports, steam ducts and other support structures in the ACSC. These models will be used for the investigation of ACSC effectiveness during windy conditions
- Investigate the effect of wind on the effectiveness of a free standing ACSC (without the placement of the building) using symmetry for two wind directions to show general flow effects occurring in the vicinity of the ACSC and recognize a performance trend.
- Investigate the effect of power station buildings on the effectiveness of the large ACSC using symmetry for the case of one wind direction.

- Subsequently the individual and combined effect of various skirt and screen configurations along the periphery and beneath the freestanding ACSC, as well as the ACSC with the building located, will be investigated.

Chapter 2

ACSC system description

2.1 Applicable system details

The two air-cooled systems investigated in this study namely, Van Rooyen (2007) and the Large ACSC, differ in a number of ways. General dimensions and layout of both these systems are shown hereafter, while heat-exchanger, fan specifications and operating conditions are given in appendix A.

2.1.1 Van Rooyen (2007) ACSC

The Van Rooyen (2007) ACSC system, depicted in figure 2.1, forms one cooling unit (provides cooling for one turbine-generator unit) and consists of an array of $5 \times 6 = 30$ fans with a series of heat-exchanger bundles in an A-type configuration downstream of the fans. For convenience the position of each fan is numbered by *(i,j)*, where i is referred to as the street (x-direction) and j the row (y-direction) in which the fan is located, if the indicated coordinate system is used.

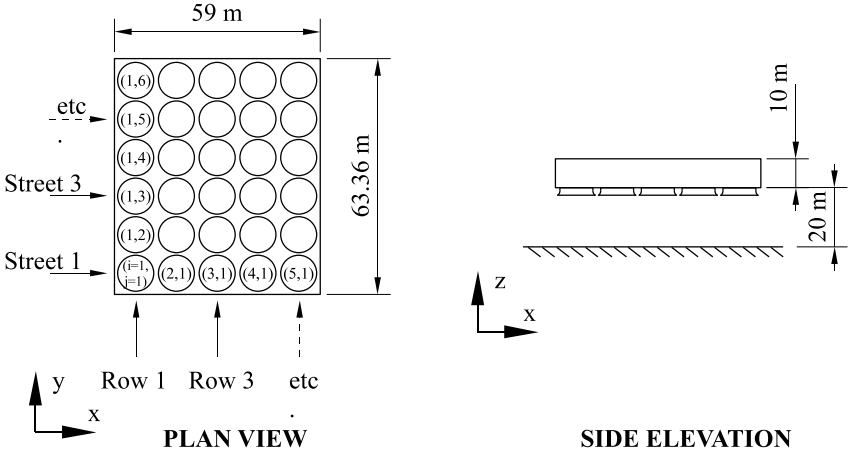

Figure 2.1: General layout and dimensions of the Van Rooyen (2007) ACSC

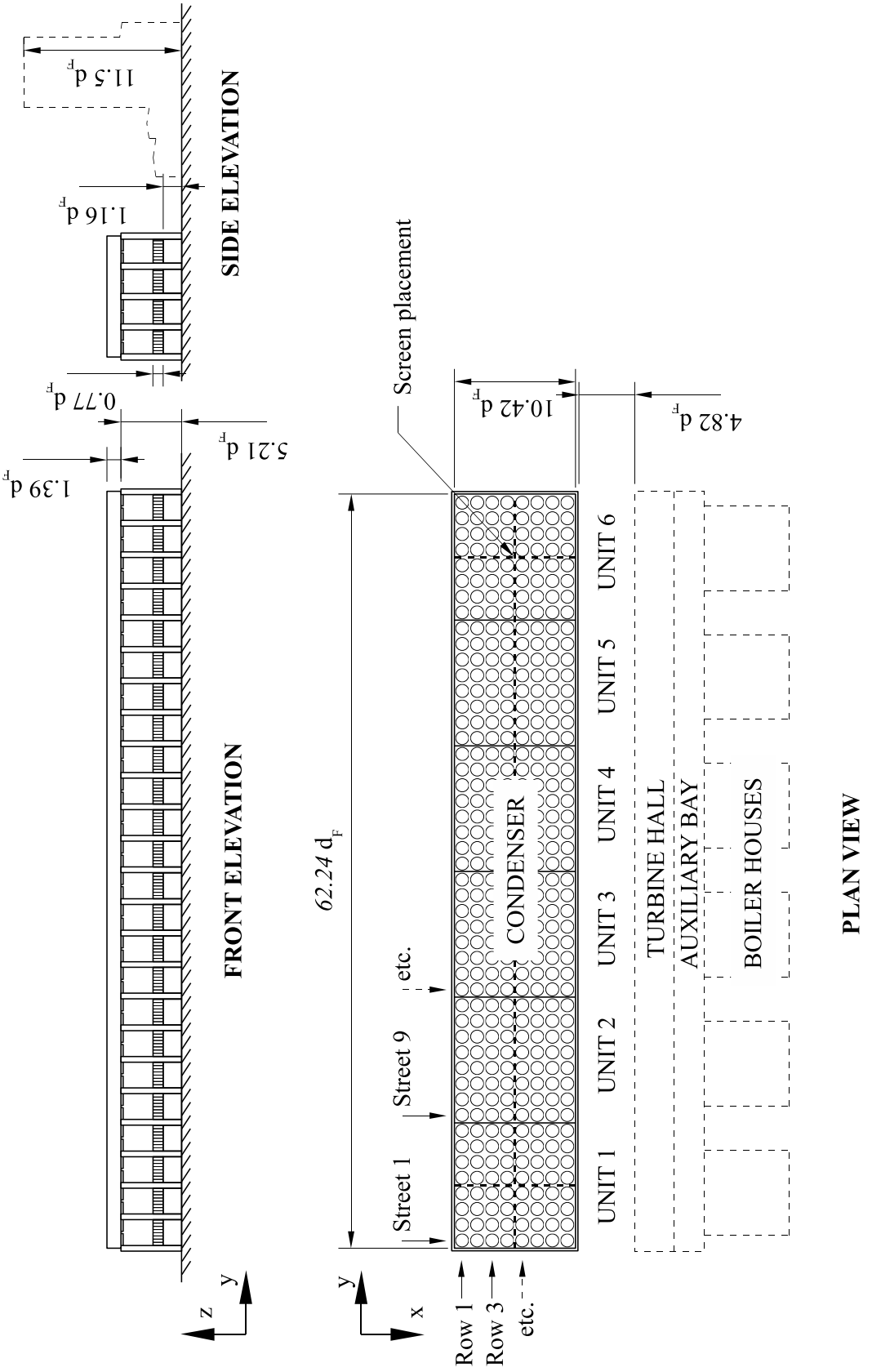

Figure 2.2: General layout and dimensions of the Large ACSC

2.1.2 Large ACSC

The general layout and dimensions of the Large ACSC is shown in figure 2.2, where 6 cooling units can be seen. Each cooling unit consists of $8 \times 8 = 64$ fans together with the heat-exchanger bundles configured in a similar manner to that described previously and serves one turbine-generator unit. Once again the specific position of a fan is numbered by *(i,j)*, where i is the street and j the row in which the fan is located.

2.2 System components

An ACSC primarily consists of an arrangement of "fan-units". One "fan-unit" consists of one fan together with a number of heat exchanger bundles. An example of a typical fan unit situated on the periphery of an ACSC is shown in figure 2.3, depicting it's main components.

During operation, an electrically driven fan draws atmospheric air upward over a wire screen and through a bell mouth inlet before it reaches the fan. Downstream of the fan, the flow is obstructed by the fan bridge, support structures and the heat-exchanger. The flow exiting the heat-exchanger is then deflected upwards into the atmosphere. Figure 2.3 also shows the placement of a windwall, which is normally fixed to the periphery of an ACSC, primarily to reduce plume recirculation.

2.2.1 Axial fan

Axial fans used in large cooling plants are unique due to their size. These fans displace large volumes of air at a relatively low pressure difference across the fan. According to Bredell (2005), aspects such as noise generation, structural strength and cost of these fans are important when large cooling plants are designed.

A scale version of these cooling fans is normally tested in a fan test facility according to one of many existing test standards such as British standard 848 (British Standard 848, 1997) or AMCA (Air Moving and Conditioning Association, (AMCA, 1975)). It needs to be noted that these tests render a fan characteristic for undistorted inflow conditions. This is not necessarily the operating condition fans are subjected to in practice, especially in ACSC's where air approaching certain fan inlets is distorted due to the effect of wind or induced cross-flow from surrounding fans (Salta and Kröger, 1995).

Two different eight-bladed fans were considered in the present study, namely the B-fan (Bruneau, 1994) for application in the Van Rooyen (2007) ACSC and

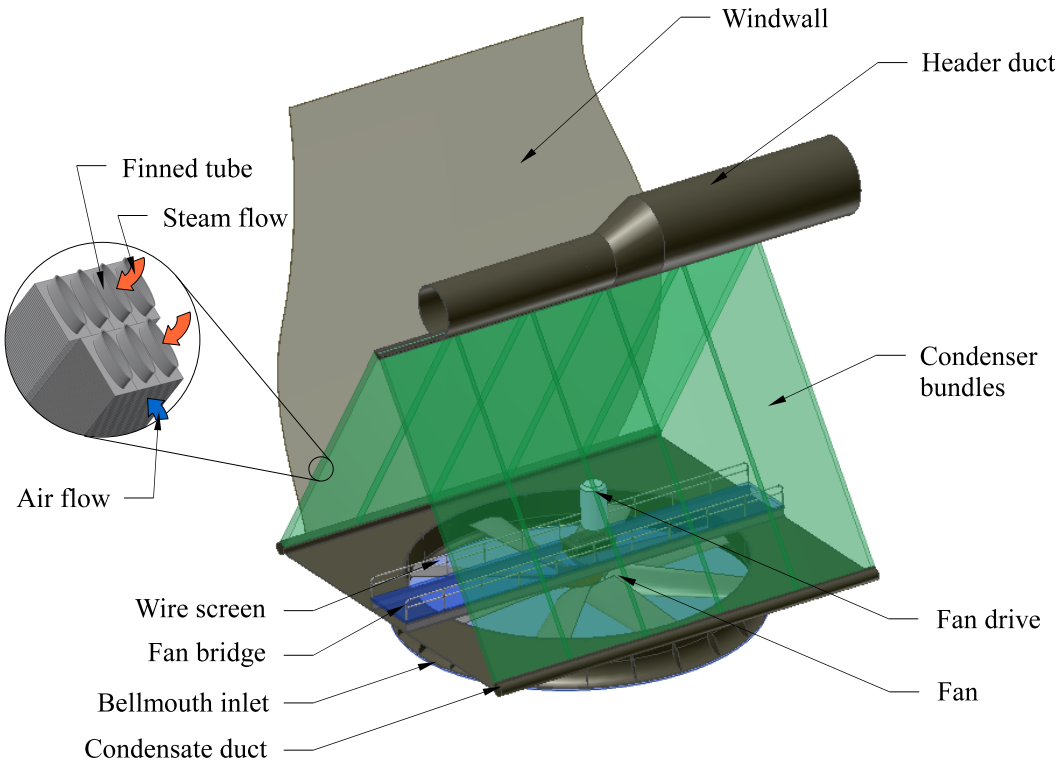

Figure 2.3: A typical ACC fan unit

a commercially available fan for the Large ACSC. Due to the confidentiality of the present study, the latter fan will be referred to as the L-fan. Fan installation specifications as well as characteristics of these fans are given in appendix A.

2.2.2 Heat-exchanger bundles

A single fan-unit consists of number of A-type configured heat-exchanger bundles downstream of the axial flow fan. These condenser bundles consist of finned tube rows, which are connected to a steam header duct at the top and a condensate drain duct at the bottom. Steam entering the finned tubes through the header duct, condenses and flows out into the condensate drain duct.

Flattened mild steel tubes with aluminum fins are used in the case of the Van Rooyen (2007) condenser, whereas elliptically cross-sectioned galvanized mild steel tubes with rectangular fins are used in the Large ACSC. The heat-exchanger bundles consist of two rows of finned tubes in a staggered arrangement, as can be seen in figure 2.3. A smaller fin pitch on the downstream (second) tube row compared to the upstream (first) tube row result in a near uniform condensation rate between these successive rows. This reduces non-

condensible gas back-flow from the downstream row to the upstream row, which is a problem commonly found in multi-row condensers (Kröger, 2004).

The heat-exchanger bundle specifications for the Van Rooyen (2007) ACSC is given in appendix A, whereas the specifications for the Large ACSC are omitted due to confidentiality.

2.3 Flow and heat transfer analysis

According to Bredell (2005) an ACSC has to condense a certain amount of steam, in order for turbine operation to occur efficiently. The cooling provided by a single fan-unit is a function of the air mass flow provided by the fan as well as the inlet air temperature to the heat-exchanger bundles. Inherently the amount of cooling provided by an entire ACSC cooling unit could therefore be quantified as the summation of the cooling provided by each fan-unit.

2.3.1 Flow calculation

The air flowing through the ACSC is subject to mechanical energy losses. Each loss can be defined by a loss coefficient, K, given as

$$K = \frac{\Delta p}{\rho v^2/2} \tag{2.3.1}$$

where v is the flow velocity based on a certain flow area.

The draft equation for a single fan unit is specified as

$$p_1 - p_7 = \frac{K_{ts}\left(\frac{m_a}{A_{tfr}}\right)^2}{2\rho_{a1}} + \frac{K_{up}\left(\frac{m_a}{A_e}\right)^2}{2\rho_{a3}} - \Delta p_{Fs} + \frac{K_{do}\left(\frac{m_a}{A_e}\right)^2}{2\rho_{a3}} + \frac{K_{\theta t}\left(\frac{m_a}{A_{tfr}}\right)^2}{2\rho_{a56}} \approx 0, \quad N/m^2 \tag{2.3.2}$$

The various loss coefficients in equation (2.3.2) are discussed in greater detail in appendix A, whereas the fan static pressure, Δp_{Fs}, is given by equation (B.1.1) in appendix B. Finally A_{tfr} and A_e is the total heat exchanger frontal area for one fan unit and the fan annulus area respectively. A_{tfr} is given for a certain ACSC system, whereas A_e is determined as follow:

$$A_e = \frac{\pi(d_c^2 - d_h^2)}{4} \quad , m^2 \tag{2.3.3}$$

where d_c and d_h are the fan casing and fan hub diameters respectively.

2.3.2 Heat transfer calculation

Heat transferred to the atmosphere was calculated using the ε-NTU method assuming the steam temperature inside the heat-exchanger bundles to remain constant. This assumption will be discussed to more detail in section 3.4.

The energy equation is given by:

$$\begin{aligned} Q_a &= \sum_{i=1}^{n_r} m_a c_{pa(i)} \left(T_{ao(i)} - T_{ai(i)}\right) \\ &= \sum_{i=1}^{n_r} \varepsilon_{(i)} m_a c_{pa(i)} \left(T_{s(i)} - T_{ai(i)}\right) \quad , W \end{aligned} \tag{2.3.4}$$

where n_r is the number of tube rows present in the heat-exchanger. Since condensation takes place inside the heat-exchanger, the effectiveness, $\varepsilon_{(i)}$, of each tube row can be calculated as follow:

$$\varepsilon_{(i)} = 1 - e^{\left(\frac{-UA_{(i)}}{m_a c_{pa(i)}}\right)} \tag{2.3.5}$$

In equation (2.3.5), the overall heat transfer coefficient, $UA_{(i)}$, for a certain row is given as

$$UA_{(i)} \approx h_a A_{(i)} = k_a A_{(i)} Ny_{(i)} P_r^{0.333} \quad , J/K \tag{2.3.6}$$

where $h_a A_{(i)}$ is the effective heat transfer coefficient for a certain tube row. The heat transfer parameter, $Ny_{(i)}$, for a specific tube row is defined by Kröger (2004) as

$$Ny_{(i)} = aRy_{(i)}^b \quad , 1/m \tag{2.3.7}$$

where a and b are constants unique to a tube row. The flow parameter, $Ry_{(i)}$, for each row is defined as

$$Ry = \frac{m_a}{\mu_a A_{(i)}} \quad , 1/m \tag{2.3.8}$$

Chapter 3

Numerical modeling

According to Versteeg and Malalasekera (2007), CFD (Computational Fluid Dynamics) could be defined as the analysis of systems involving (but not confined to) fluid flow and heat transfer by means of computer simulation. This section gives a brief overview of the governing equations of a fluid in motion. It also looks into discretization, solver settings, turbulence and buoyancy modeling and boundary conditions applicable to this thesis. Further aspects such as the modeling procedures used and the means by which ACSC performance were measured, are also discussed.

As mentioned in chapter 1 only a limited amount of computational resources were available. Modeling was done on a computer with two 3.16 GHz processors, 8 GB of RAM available and a 660 MHz graphics processing unit. Solving was maainly done on a computer cluster. Each computing node on the cluster has eight 2.83 GHz processors, with 16 GB of RAM available. The largest computational domain, $\approx 12(10)^6$ control volumes, in the present study took between 8 and 12 hours to complete between 900 and 1200 iterations, if it was solved in parallel across 8 processors on the cluster. The biggest limitation occured on the computer where modeling took place. A rule of thumb commonly used for meshing is to stick to a million control volumes per 1 GB of RAM. Pushing the boundaries of the model to $\approx 12(10)^6$ control volumes, consumed all resources on the modeling computer and often corupted the modeling program GAMBIT. A typical FLUENT case and data file would also take approximately 30 minutes to open on this computer and take additional time to plot results, depending on how many the user would like to view. Taking the large amount simulations done in the present study into account, made the long waiting periods for the computer to process data impractical. Full 3D modelling of the entire power station were thus not suitable in the present research.

3.1 CFD code summary

3.1.1 Governing equations

The numerical analysis of the ACSC's under investigation was modeled with computer software, *Fluent 12*, which uses a finite volume solution technique to solve the flow field. Each volume is subject to the governing equations of fluid in motion. The steady state, three-dimensional governing equations of a fluid in motion, as found in Versteeg and Malalasekera (2007), are given below:

Continuity:

$$\text{div}(\rho \mathbf{u}) = 0 \tag{3.1.1}$$

x-momentum:

$$\text{div}(\rho u \mathbf{u}) = -\frac{\partial p}{\partial x} + \text{div}(\mu \text{ grad } u) + S_{Mx} \tag{3.1.2}$$

y-momentum:

$$\text{div}(\rho v \mathbf{u}) = -\frac{\partial p}{\partial y} + \text{div}(\mu \text{ grad } v) + S_{My} \tag{3.1.3}$$

z-momentum:

$$\text{div}(\rho w \mathbf{u}) = -\frac{\partial p}{\partial z} + \text{div}(\mu \text{ grad } w) + S_{Mz} \tag{3.1.4}$$

Energy:

$$\text{div}(\rho i \mathbf{u}) = -p \text{ div } \mathbf{u} + \text{div}(k \text{ grad } T) + \Phi + S_e \tag{3.1.5}$$

The velocity vector $\mathbf{u}$ is defined as

$$\mathbf{u} = u + v + w \tag{3.1.6}$$

where u, v and w are the velocities in the x, y and z directions respectively when a cartesian coordinate system is used.

The momentum source terms, S_{Mx}, S_{My} and S_{Mz}, account for all external momentum sources such as buoyancy and gravitational forces in the fluid. These source terms also account for other obstructions in the flow path typically modeled by porous media (Fluent Inc., 2006).

According to Versteeg and Malalasekera (2007) all effects due to viscous stresses in the energy equation can be taken into account by the dissipation function, Φ, defined as

$$\Phi = \mu\Bigg\{2\left[\left(\frac{\partial u}{\partial x}\right)^2 + \left(\frac{\partial v}{\partial y}\right)^2 + \left(\frac{\partial w}{\partial z}\right)^2\right] + \left(\frac{\partial u}{\partial y} + \frac{\partial v}{\partial x}\right)^2 + \left(\frac{\partial u}{\partial z} + \frac{\partial w}{\partial x}\right)^2 + \left(\frac{\partial v}{\partial z} + \frac{\partial w}{\partial y}\right)^2\Bigg\} - \frac{2}{3}\mu(\text{div } \mathbf{u})^2 \tag{3.1.7}$$

Lastly the source term, S_e, in the energy equation accounts for additional volumetric heat sources e.g. chemical reactions or heat transfer, other than conduction or convection between neighboring cells.

3.1.2 Discretization and solver settings

The commonalities in the governing equations enables the definition of a general transport equation in terms of variables, ϕ and Γ. The general transport equation is expressed as:

$$\text{div}(\rho\phi\mathbf{u}) = \text{div}(\Gamma \text{ grad } \phi) + S_\phi \tag{3.1.8}$$

The governing equations can be obtained by setting ϕ equal to 1, u, v, w and i respectively, and selecting the corresponding values for the diffusion coefficient, Γ. According to Versteeg and Malalasekera (2007), equation (3.1.8) is the starting point of any numerical calculation in the finite volume method and needs to be integrated (discretized) for individual control volumes in the computational domain.

The value, ϕ, of an individual volume, is stored at the center of the volume (Fluent Inc., 2006) and requires the solution of the discretized equation, unique to that volume. However, to solve the discretized equation, requires the substitution of boundary conditions, ϕ_f, obtained at the volume faces. These boundary conditions are calculated by means of a differencing or interpolation scheme between ϕ of neighboring volumes. Consequently, some iteration is required in order to obtain ϕ.

Numerical computation in the present study was done using a first order upwind differencing scheme. According to Fluent Inc. (2006), this scheme is computationally more stable compared to the second order upwind scheme. This advantage does however come at the expense of reduced accuracy and could lead to problems such as numerical diffusion. The first order upwind scheme does however always render a realistic solution, making it an appropriate choice for the present study, since a performance *trend* is investigated.

Gradients, $\nabla\phi$, were calculated using Green-Gauss node based gradient evaluation. This method provides second order accuracy in the evaluation of gradients between the nodes on volume faces and is the preferred method when unstructured grids are solved (Fluent Inc., 2006).

Pressure-velocity coupling was done using the SIMPLE algorithm, since it provides superior convergence for grids containing skew cells (Fluent Inc., 2006) and is therefore suitable for the unstructured grids implemented in the present study.

3.1.3 Turbulence modeling

All flow encountered in engineering can be characterized as turbulent or laminar depending on the level of chaos present in the flow, which is an indication of the random variation of local velocity and pressure in the fluid. Various turbulence models exist for numerical analysis of which individual models are relevant to different types of flow problems.

Arguably the *Standard k-ε* turbulence model is the most popular and widely used model in numerical computation. Despite its many advantages, such as simplicity and countless validation, the *Standard k-ε* turbulence model shows poor performance in predicting swirling and rotating flows (Versteeg and Malalasekera, 2007). For this reason some variations of the *Standard k-ε* model was developed.

According to Fluent Inc. (2006) the *Realizable k-ε* model provides superior performance in flows where rotation, separation and recirculation is present. Joubert (2010) also investigated the effect of wind on the performance of the Van Rooyen (2007) ACSC using the *Standard*, *RNG* and the *Realizable k-ε* model. The study showed a negligible difference between the respective numerical results.

The *Realizable k-ε* model is used for the present numerical calculation of turbulence in the vicinity of an ACSC.

3.1.4 Buoyancy modeling

Heated air rejected to the atmosphere is subject to a change in density and consequently some buoyancy modeling is required. *Fluent* provides a couple of options to buoyancy modeling. The first option solves the local density of each control volume in relation to the temperature of the volume. This might be a more accurate approach, but is expensive since solution convergence takes longer (Fluent Inc., 2006). The second option to buoyancy modeling is by means of the Boussinesq model discussed hereafter.

The Boussinesq model (equation (3.1.9)) treats density as a constant in all equations, except for the buoyancy term in the momentum equations.

$$\rho = \rho_0(1 - \beta(T - T_0)) \tag{3.1.9}$$

where ρ_0 is the operating density, T the local temperature, T_0 the operating temperature and β the thermal expansion coefficient defined as a function of the ambient temperature:

$$\beta = 1/T \tag{3.1.10}$$

According to Fluent Inc. (2006) the use of the Boussinesq model provides quicker convergence than the temperature-density relation approach, but is only valid if

$$\beta(T - T_0) \ll 1 \tag{3.1.11}$$

In the present study the largest value of the term on the right-hand side of equation (3.1.11) is calculated to be 0.089, which consequently justifies the use of the Boussinesq model.

3.1.5 Boundary conditions

The computational domain is governed by the equations specified earlier, but also has to satisfy constants set by boundaries in the flow domain. Different types of boundary conditions exist, but can mainly be classified as surface and volume based boundaries. The various boundaries used in this study are discussed hereafter.

Wall boundaries are surfaces in the computational domain with zero porosity to flow. *Fluent* enforces a default "zero-slip" condition at the fluid wall interface, but also allows the user to model a "slip-wall", by changing the default wall viscous stress settings.

Velocity boundaries allows the user to specify a fixed velocity of fluid (therefore a fixed mass flow) flowing into the computational domain (whether constant or based on a velocity profile) together with other properties such as gage pressure and temperature. Where it is necessary, it can also be used to model the rate of fluid leaving the computational domain, by specifying an outlet velocity.

Pressure boundaries require the specification of fluid pressure and are used where the profile of fluid crossing the boundary is unknown. Fluid is allowed to enter or leave the computational domain across this boundary depending on the state of the flow close to the boundary. Fluid entering the computational domain is subject to predefined properties, such as temperature and turbulence.

Fan boundaries were modeled using the *pressure-jump* method, derived in appendix B. This method uses the velocity values in the control volumes immediately upstream of the fan rotation plane to calculate a pressure difference based on the user specified fan characteristic polynomial. The pressure increase is then added to the control volumes immediately downstream of the fan rotation plane.

Symmetry boundaries are located in numerical models, where the physical geometry and the flow pattern of the numerical model is expected to have symmetry. No user specifications are required for symmetry boundaries other than the correct boundary placement.

Interior boundaries are planes inside the computational domain, bearing a certain reference tag specified by the user. These boundaries are numerically "transparent" and do not affect the flow in any way, but could however be switched to another boundary condition by the user, without altering the grid volumes.

Radiator boundaries are referenced planes, similar to *interior* boundaries, yet these boundaries allow the user to specify a pressure difference and heat transfer coefficient as functions of the normal velocity to the identified radiator plane.

Porous media is a boundary condition applied to a zone of identified volumes in the computational domain and allows the user to alter the flow in this zone, by specifying energy and momentum source terms. It could be used to simulate the flow through packed beds, flow distributers or any other volumetric obstacle.

3.2 Modeling of a single fan unit

As mentioned in section 2.2, an entire ACSC consists of a number of individual fan-units. The summation of individual fan-unit performances would consequently give the performance of the entire ACSC. It is therefore necessary to create a numerical fan-unit model that would accurately solve the flow and heat transfer through a fan unit, at a reasonable computational expense.

The numerical modeling of a conventional A-frame fan unit as depicted in figure 3.1 (a), poses some computational challenges since details such as the inlet screen, fan bridge and other obstructions to flow, require a fine computational grid. In addition to this, the explicit modeling of the fan and heat-exchanger bundles also holds some computational complexities. Since the main aim of this thesis is to investigate a performance trend of an ACSC and not the flow through the plenum chamber, such detail could be modeled with less effort by implementing a simplified fan-unit model similar to the model proposed by Bredell (2005) and shown in figure 3.1 (b).

Dimensions to the simplified fan-unit model (figure 3.1 (b)) are given in table 3.1. This simplified fan-unit consists of a heat-exchanger and fan model, placed in the xy-plane. Both these models will be discussed hereafter.

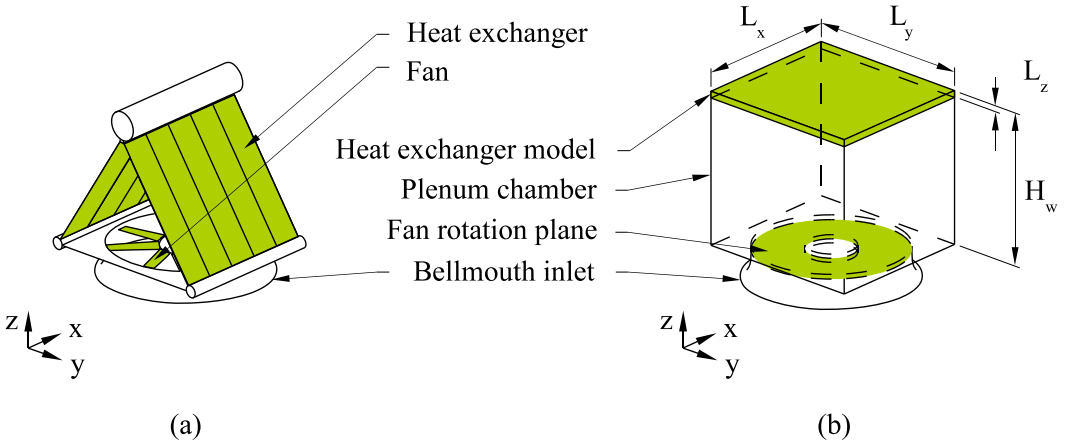

Figure 3.1: Representation of a conventional A-frame fan-unit and its corresponding numerical model

Table 3.1: Simplified fan-unit dimensions

System	H_w, m	L_x, m	L_y, m	L_z, m
Large ACSC	14.4	13.5	13.625	0.2
Van Rooyen (2007)	10	11.8	10.56	0.2

3.2.1 Heat-exchanger model

As can be seen in figure 3.1 (b), detail such as supports, wire screens, fan bridges, finned tube bundles and additional support structures are absent in the numerical fan-unit model. Furthermore, the rectangular plenum chamber is different to the A-configuration of the fan-unit in practice, resulting in a different flow path through the fan-unit.

The one-dimensional draft equation (equation (2.3.2)) presented by Kröger (2004), does however provide a method to calculate the effective system resistance, Δp_e, of a single fan-unit, if the Δp_{Fs} component is omitted. This equation accounts for the mechanical flow losses due to the obstructions mentioned previously as well as the flow effects, such as contraction, expansion and jetting.

Since all flow through a conventional fan-unit is eventually deflected upward into the atmosphere, a rectangular plenum fan-unit model could be used with a downstream porous zone, where the porous zone accounts for the effective flow resistance through the fan unit. Moreover, a comparison was done by Owen (2010) between an A-frame and a simplified fan-unit model and showed

that there exists a minimal difference in volumetric effectiveness between the respective models.

The calculation of a Van Rooyen (2007) fan-unit effective system resistance is shown in appendix A. A similar calculation for a *Large* ACSC fan-unit is omitted due to confidentiality.

The porous zone in *Fluent* accounts for the flow resistance by means of momentum source terms, S_i, added to the momentum equations and is given as:

$$S_i = -\left(\frac{\mu}{\alpha_i}u_i + C_i\frac{1}{2}\rho|\mathbf{u}|u_i\right) \quad , N/m^3 \tag{3.2.1}$$

where the footnote, i, represents the individual cartesian directions, x, y or z. C_i and $1/\alpha_i$ are the inertial and viscous loss coefficients, respectively and should be specified by the user. The primary flow direction through the numerical heat-exchanger is upward (z-direction). Consequently the resistance to flow must be in the opposite direction.

The z-direction inertial and viscous loss coefficients for a Van Rooyen (2007) fan-unit are calculated in appendix C.1. Once again a similar calculation for a single Large ACSC fan-unit is omitted due confidentiality. The inertial and viscous coefficients for the heat-exchanger model of a Van Rooyen (2007) fan-unit are conveniently repeated in table 3.2, but omitted for a Large fan-unit.

Table 3.2: Inertial and viscous loss coefficients

System	$\boldsymbol{C_z, m^{-1}}$	$\boldsymbol{1/\alpha_z, m^{-2}}$
Large ACSC	a	b
Van Rooyen (2007)	59.5447	$2.440231(10)^6$

The porous zone in *Fluent* also allows the user to specify a volume based heat source term, S_e, as shown in equation (3.2.2), to model heat transfer. This term was calculated as shown in appendix C.2 and added to the discretized energy equations of the control volumes in the porous zone by means of a user defined function (UDF).

$$S_e = \frac{\delta Q}{\delta V} = \frac{\rho_a|w|}{L_z}c_{pa}\left(T_{ao} - T_{ai}\right) \quad , W/m^3 \tag{3.2.2}$$

3.2.2 Fan model

The numerical modeling of fans could be done in various ways of which two methods, namely *actuator-disk* and *pressure-jump* methods will be discussed hereafter.

The *actuator-disk* numerical fan model developed by Thiart and Von Backström (1993) calculates momentum source terms based on blade element theory, applicable to flow through the fan. These source terms are then added to the momentum equations relevant to the control volumes in the fan model. This model has successfully been implemented in previous studies by researchers such as Duvenhage *et al.* (1995), Bredell (2005), Van Rooyen (2007) and Van der Spuy *et al.* (2009).

The *pressure-jump* fan model is the default model available in *Fluent* and can simulate flow relatively accurately with a reduced number of control volumes in the vicinity of the fan allowing the user to solve an array of fans simultaneously (Van der Spuy *et al.*, 2009). This model gives a static to static pressure rise to the control volumes immediately downstream of an infinitely thin fan plane, based on a user specified fan characteristic polynomial (Fluent Inc., 2006).

As mentioned in section 1.2, Van Rooyen (2007) investigated the effect of wind on an ACSC using the *actuator-disk* model. The same ACSC was also investigated by Owen (2010) and Joubert (2010) who both verified the performance trends of Van Rooyen (2007), but implemented the *pressure-jump* fan model. Van der Spuy *et al.* (2009) investigated the difference in fan performance obtained by means of the *actuator-disk* and *pressure-jump* model for typical fan operation in a large ACSC. This study also revealed a marginal difference in fan performance between the two models, but it did not show a comparison for low air flow rates through the fan.

The above-mentioned literature suggests that the *pressure-jump* model is acceptable for normal inflow and renders results that are comparable to results obtained by the *actuator-disk* model for distorted inflows. However literature is vague regarding the accuracy of both these models for highly separated (radial) flow at the fan inlet and extremely low volume flows.

Due to the uncertainty of the mentioned fan models and the greater amount of computational power required to solve a large number of fans using the *actuator-disk* model, a decision was made to implement the *pressure-jump* model for the present study. This decision is justified as follow:

- The number of fans affected by separated flow are limited. Using the

pressure-jump model would therefore lead to a relatively accurate estimation of an overall ACSC performance trend.

- The limit in computational resource favors the use of the *pressure-jump* model, since it requires fewer control volumes in the vicinity of the fan compared to the *actuator-disk* model.

The *pressure-jump* fan polynomials were derived from the original total to static characteristic pressure curves, provided by the fan supplier, as shown in appendix B. The polynomial for the Van Rooyen (2007) ACSC is repeated in table 3.3 for convenience, but omitted for the case of the Large ACSC due to confidentiality.

Table 3.3: *Pressure-jump* fan characteristic polynomials

System	$\boldsymbol{\Delta p_{Fss}, N/m^2}$
Large ACSC	$c_1 v^2 + c_2 v + c_3$
Van Rooyen (2007)	$-2.63055v^2 + 27.2461v + 323.2303$

3.2.3 Single fan-unit grid

The grid used to calculate the flow through a single fan unit is depicted in figure 3.2. The grid on the fan face is shown in figure 3.2 (c). An unstructured tetrahedral grid was chosen for the modeling procedure discussed in section 3.3. This grid type provides good accuracy and has the ability to "grow" or "shrink" in all three cartesian directions, depending on where greater accuracy is required in the computational domain.

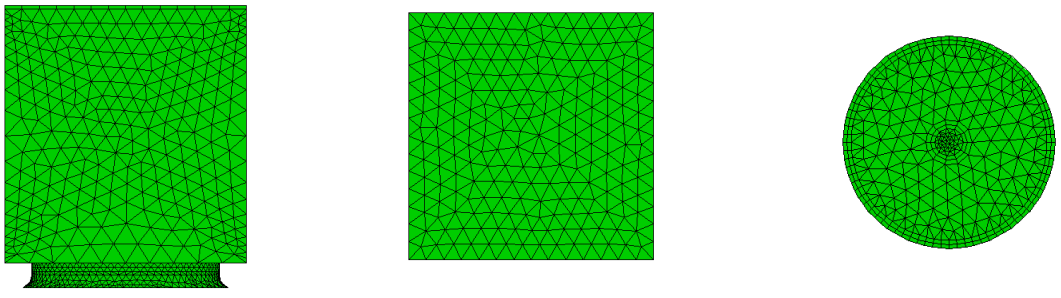

(a) (b) (c)

Figure 3.2: Computational grid for a single fan-unit

The heat-exchanger model, consists of wedge shaped control volumes. This is a requirement for the UDF, calculating the heat transfered by the heat-exchanger model. The UDF extracts the velocities from *Fluent* on the upstream face of the heat-exchanger model and calculates the corresponding heat source terms. These terms are consequently added to the control volumes in the heat-exchanger model.

Some control volumes would not have a surface situated on the upstream face of the heat-exchanger model if tetrahedral cells were used for this purpose. This would lead to some cells in the heat-exchanger model not receiving a heat source term, which is an inaccurate approximation to the heat transferred.

Other grid and boundary specifications, applicable to a single fan-unit are listed hereafter:

- A boundary layer grid was placed on the fan side of the bellmouth inlet as well as around the hub face (figure 3.2 (c)) to simulate any effects of a boundary layer if it should exist.
- The walls of the plenum chamber were modeled as slip-walls (zero friction at the fluid-wall interface), since this is not part of the fan-unit in practice and no mechanical energy losses will occur due to these walls.
- A zero slip condition was applied to the bellmouth faces, since no mechanical energy losses due to this obstruction are taken into account by equation (2.3.2).
- Finally the hub was modeled as a flat face with a zero slip wall boundary condition for the case of the *Large* ACSC fan-unit, since the effect of the true hub were regarded to be negligible in the overall fan-unit performance. This is also justified, since some uncertainty exists regarding the fan model and therefore the detailed modeling of the hub, could be excessive. A different hub is fitted in the B-fan used for the Van Rooyen (2007) ACSC, and was modeled in the same manner.

The heat transfer and flow of a single fan-unit was investigated analytically and verified through numerical investigation. This flow through the fan-unit is referred to as the ideal volume flow rate, V_{Fid}, and will be discussed in section 4.1. The computational domain for thermo-flow investigation of a single fan-unit is shown in figure 3.3, depicting all dimensions and domain boundaries. The height of the fan-unit above ground level, H_i, is unique to each system evaluated in the present study and is given in appendix A.

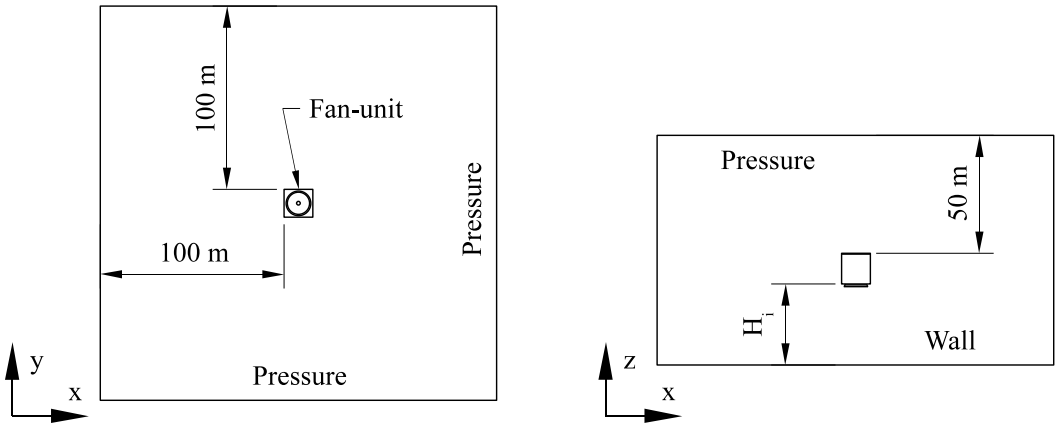

Figure 3.3: Computational domain for validation of a single fan-unit

3.3 Modeling procedures

Modeling of the *Large* ACSC poses some difficulty, since flow in the vicinity of the ACSC is complicated (vortex shedding and distorted flow), consequently requiring a detail computational grid. For this reason various modeling procedures were investigated in an attempt to reduce the amount of computational power required to solve the flow around and through the ACSC's applicable to the present study. Symmetry was used to model the ACSC in order to save on computational requirements together with the *Iterative* modeling procedure discussed hereafter.

3.3.1 Modeling of wind

Wind blowing across the ACSC was modeled by means of a flow distribution at the velocity inlet to the computational domain. This distribution is specified by means of the velocity profile given by:

$$v_z = v_{ref}\left(\frac{z}{z_{ref}}\right)^b \quad , m/s \tag{3.3.1}$$

where v_z is the horizontal velocity magnitude at height, z and v_{ref} is the reference velocity at platform height, $z_{ref} = H_i$.

The coefficient, b, is given in table 3.4 for the individual systems under investigation in the present study. It should be noted that 1/7 was used for investigation of the Van Rooyen (2007) ACSC. A b-coefficient of 1/5, as recommended by VDI (1978), was used in the present study for the large ACSC.

Table 3.4: b-coefficients for wind profiles

System	b
Large ACSC	1/5
Van Rooyen (2007)	1/7

3.3.2 Modeling procedure for the Van Rooyen (2007) ACSC

The computational domain used to model the effect of an x-direction wind on the performance of the Van Rooyen (2007) ACSC is shown in figure 3.4. This figure depicts the specific dimensions as well as different boundary conditions applied to the domain outer boundaries. Modeling of the ACSC was done with an array of numerical fan-units, discussed previously. Symmetry was used to reduce the computational effort required to solve the grid.

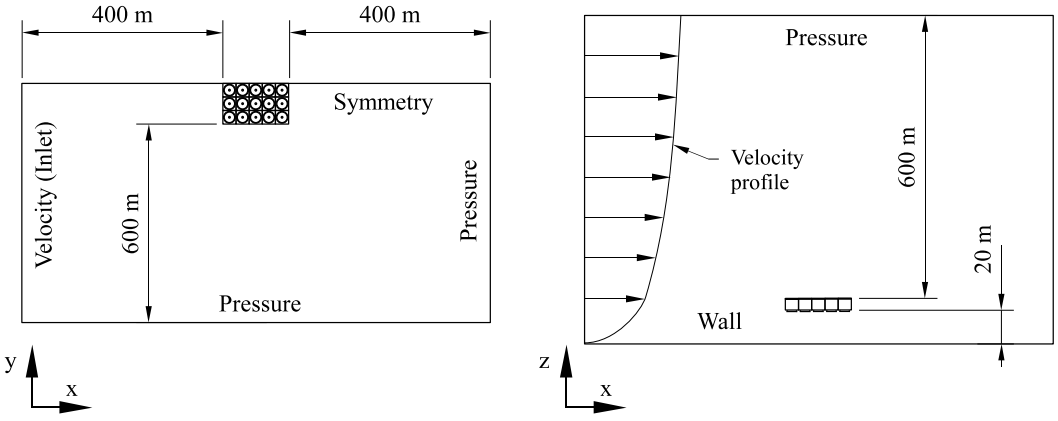

Figure 3.4: Computational domain for calculation of the flow around and through the Van Rooyen (2007) ACSC

The computational grid on the symmetry plane is shown in figure 3.5. The entire grid consists of $4.9(10)^6$ tetrahedral volumes. These volumes are concentrated in the vicinity of the ACSC model (figure 3.5 (b)) and grow larger in all three cartesian directions towards the domain outer boundaries. The volumes at the bottom of the domain inlet are also concentrated, since the horizontal velocity magnitude in the z-direction changes rapidly in this region, due to the inlet velocity profile.

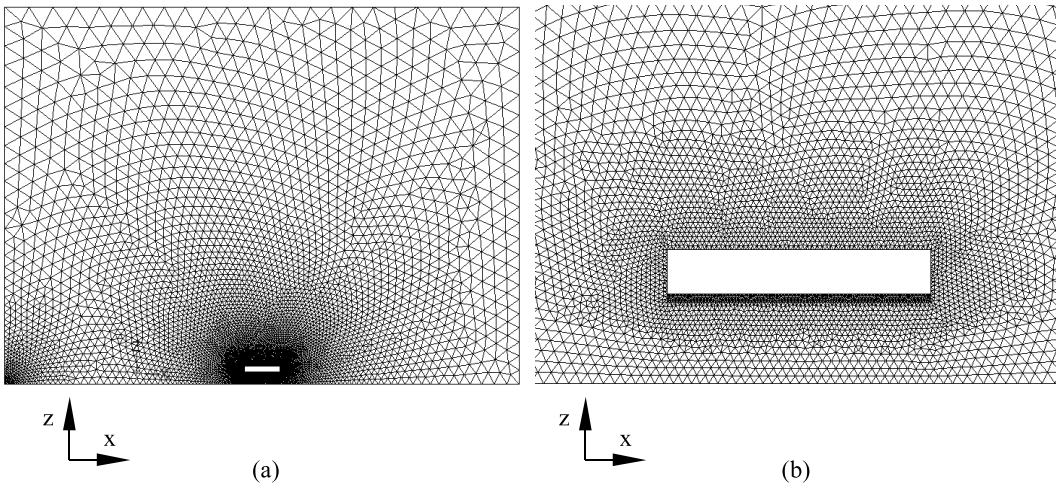

Figure 3.5: Computational grid for calculation of the flow around and through the Van Rooyen (2007) ACSC

After all solver settings and boundary conditions were applied to the computational grid, solving commenced to the point where the volumetric flow rate, V_F, through all fans converged such that $|V_{Fprevious} - V_{Fcurrent}| < 0.1$ m^3/s.

3.3.3 *Iterative* modeling procedure for the Large ACSC

An *Iterative* modeling procedure was used to generate results for the Large ACSC in the present study. This subsection is focused on the description of the *Iterative* modeling procedure. This modeling procedure is validated hereafter in chapter 4.

Different computational domains were required to model the effect of positive x-direction and y-direction winds, due to the difference in symmetry between these two cases. This was done using the computational domains, seen in figure 3.6 (a) and (b) respectively.

Details of the x- and y-direction condenser models in these computational domains are shown in figures D.1 and D.2 of appendix D, respectively. These figures show the placement of fan-units in the ACSC model, the position of the ACSC model velocity boundaries as well as the position of various skirts and screens. The aforementioned were modeled by interior boundaries (hence the dotted lines in the figures) and could be switched to wall boundaries when necessary. This is advantageous for the comparison of results. The control volumes in the vicinity of the ACSC would change if a new grid was required for each of the different configurations of skirts and screens to the ACSC model. The difference in results obtained between different simulations are therefore

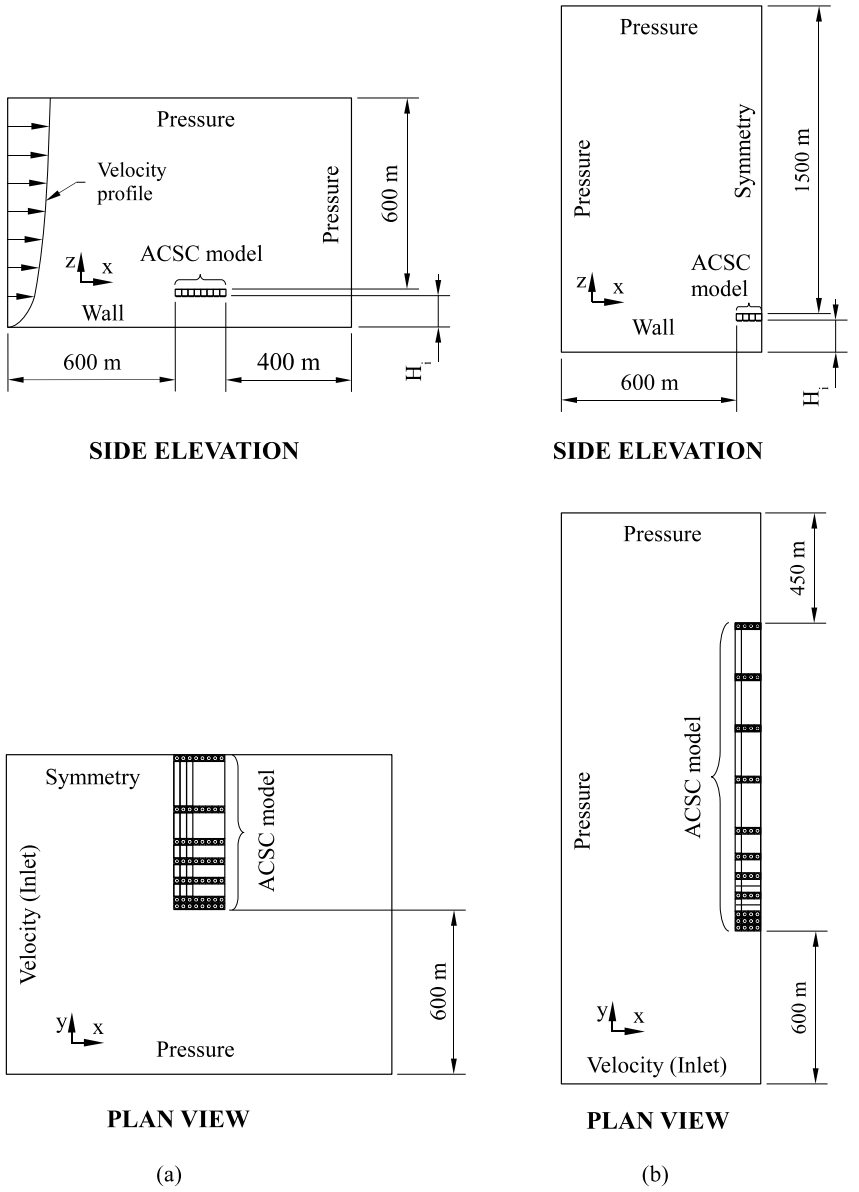

Figure 3.6: Computational domains for calculation of the flow around and through the *Large* ACSC by means of the *Iterative* modeling procedure for a (a) positive x-direction and (b) positive y-direction wind

purely due to the effect of the mentioned modifications.

The grid for both the positive x- and y-direction wind domains consist of $8.3(10)^6$ and $11.8(10)^6$ tetrahedral control volumes respectively. Once again the volumes are concentrated around the ACSC model and grow larger toward the domain outer boundaries. The grid on the symmetry plane of the positive x- and y-direction domains are shown respectively in figure 3.7 (a) and (b).

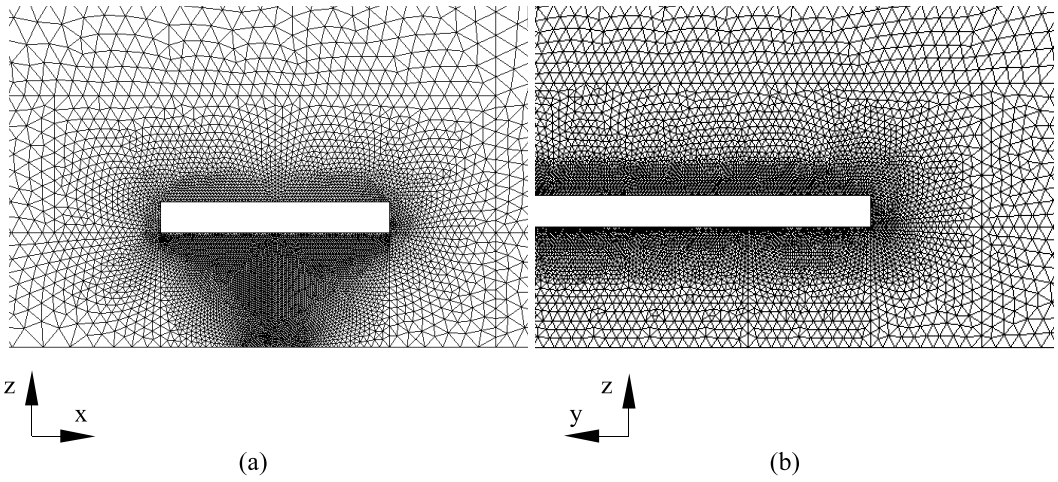

Figure 3.7: Computational grids for calculation of the flow around and through the *Large* ACSC by means of the *Iterative* modeling procedure

The *Iterative* modeling procedure is discussed using figure 3.8 as reference.

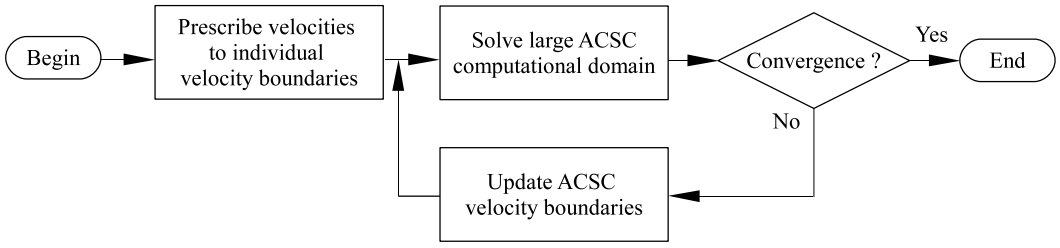

Figure 3.8: *Iterative* numerical procedure

Wind blowing across the ACSC is simulated by means of a velocity profile, applied to the domain inlet. The velocity boundaries, forming part of the ACSC, have a specified velocity that is based on the average volumeflow between the two fan-units located on the adjacent sides of the velocity boundary in the y-direction, and are calculated as shown in figure 3.9 and given by:

$$v_{vb(i)} = \frac{\frac{1}{2}\left(V_{f(a)} + V_{f(b)}\right)}{A_e} \quad ,m/s \tag{3.3.2}$$

where, i is the face between fan-units a and b, and A_e the effective flow area of a single fan-unit given by equation (3.3.3).

$$A_e = L_x \cdot L_y \quad ,m^2 \tag{3.3.3}$$

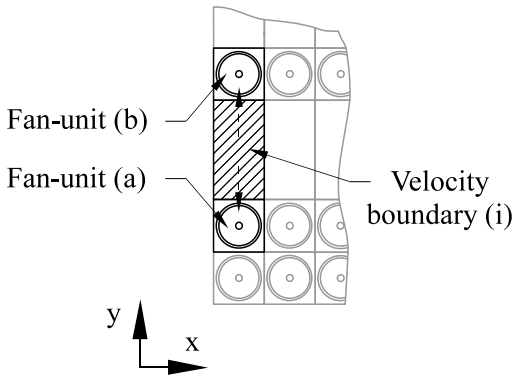

Figure 3.9: Depiction of scheme used to calculate the velocity through velocity boundaries in the ACSC model

where L_x and L_y are given in table 3.1.

Velocities, based on ideal flow conditions through a single fan-unit, are applied to the velocity boundaries in the ACSC as a first approximation. Upon convergence of the volume flow through all individual fan-units, another simulation is done where the velocities through the velocity boundaries are updated for a next simulation. This process was then repeated until the volume flow through individual fans between consecutive simulations have converged.

3.4 Presentation of performance results

The purpose of the present study is to investigate the performance of a condenser. It is therefore necessary to identify sensible ways to present performance data in order to provide comparable information. This was done by quantifying performance data in two forms of a performance effectiveness, discussed hereafter.

3.4.1 Volumetric effectiveness

The volumetric effectiveness of the flow rate through individual fan-units is specified as

$$\varepsilon_V = \frac{V_F}{V_{Fid}} \tag{3.4.1}$$

where V_F and V_{Fid} is the volume flow rate through an individual fan during operating conditions in the ACSC and under ideal conditions respectively. The volumetric effectiveness of flow through a fan points out locations in the ACSC

where separation and through-flow beneath the fan platform are reducing the air flow through the fan.

The volumetric effectiveness of fans not modeled was determined using the linear interpolation scheme between adjacent fan units that were modeled. This interpolation scheme is verified in appendix E.

3.4.2 Heat transfer effectiveness

As previously mentioned, heat transfer calculation of a single fan-unit is done using the ε-NTU method given by equation (3.4.2), where an average steam temperature is used in the finned tubes.

$$Q = \varepsilon m_a c_{pa}(T_s - T_{ai}) \quad , W \tag{3.4.2}$$

Consequently a heat transfer effectiveness, shown in equation (3.4.3), would indicate the performance of a fan-unit. This performance is the amount of heat transferred to the air by a single fan unit under certain operating conditions of the ACSC, Q_F, compared to ideal operating conditions, Q_{Fid}, of a single fan-unit.

$$\varepsilon_{Q_F} = \frac{Q_F}{Q_{Fid}} \tag{3.4.3}$$

The overall heat transfer effectiveness of an ACSC unit, ε_{Q_U}, can therefore be expressed as:

$$\varepsilon_{Q_U} = \frac{\sum_{i=1}^{n_F} \varepsilon_{Q_F(i)}}{n_F} \tag{3.4.4}$$

where i accounts for the number of fan-units, n_F, in a single ACSC unit.

Chapter 4

Validation of numerical analysis

Considering that the present investigation involves the flow around an ACSC located in an atmospheric environment, uncertainty arises regarding the effect of domain boundary proximity, grid density and the effect of turbulence models on the final numerical answer. Consequently some validation is required in order to justify the results obtained by the numerical models used in the present study. This section is dedicated to the various validations that were done, providing information on the accuracy of the numerical models.

4.1 Validation of an independent fan-unit

As mentioned in chapter 3, a numerical model was used to model the flow through a single fan-unit. Validation of a single fan-unit was done by comparing the analytically obtained values for the air volume flow through the fan and the air outlet temperature leaving the fan-unit, to the computational results obtained for the numerical fan-unit model.

4.1.1 Volumetric flow rate

The ideal volumetric flow rate, V_{Fid}, mentioned previously is taken as the amount of flow through a single free standing fan-unit under the design atmospheric conditions given in appendix A. The flow through a single fan-unit can analytically be calculated using the draft equation (2.3.2). This equation was used to calculate the fan-unit resistance to flow and is plotted in figure 4.1 for the fan-unit used in the Van Rooyen (2007) ACSC, but once again omitted in the case of the Large ACSC due to confidentiality. The intersection of the resistance and fan characteristic curves, presents the operating point of a single fan-unit.

The flow through the Van Rooyen (2007) and Large ACSC fan-units were numerically investigated as discussed in section 3.2. A comparison between the

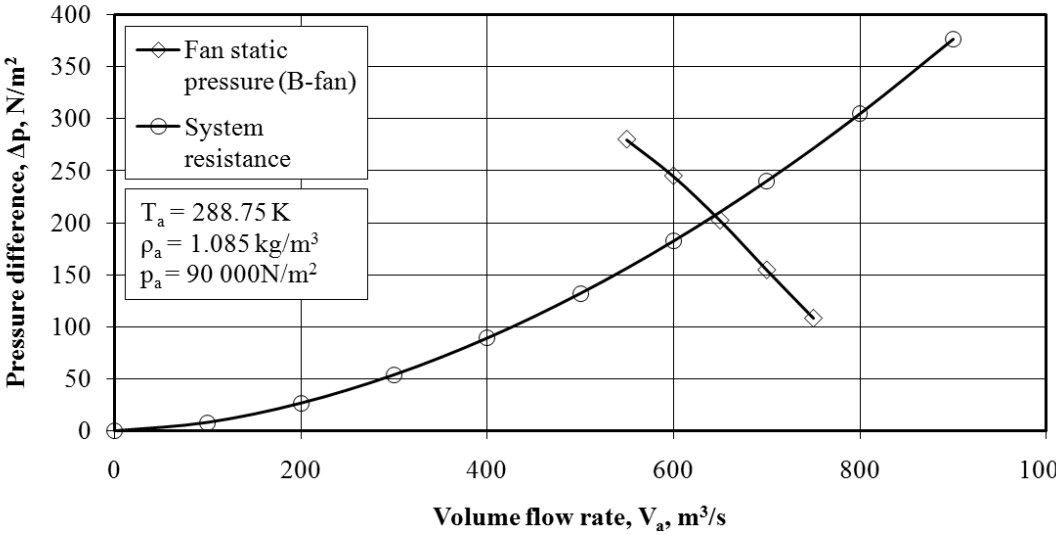

Figure 4.1: Operating point of a Van Rooyen (2007) fan-unit

analytical and numerical results obtained for the flow through both fan-units is given in table 4.1

Table 4.1: Comparison between analytical and numerical values for the ideal volumetric flow operating point

	$V_{Fid}, m^3/s$	
System	**Analytical**	**Numerical**
Large ACSC	701.68	706
Van Rooyen (2007)	645.79	640

A good correlation can be seen between the analytical and numerical results, showing that the fan and numerical resistance is appropriate for use in this study.

4.1.2 Heat transfer

As mentioned previously, heat transferred by a fan-unit to the atmosphere was modeled by means of a UDF. The UDF would extract information from *Fluent* and use this to calculate the heat transfer source term as shown in appendix C. The calculation requires two sets of information to be extracted from *Fluent*, namely the velocity through the control volumes and the air inlet temperature upstream of the heat-exchanger model.

Two methods of air inlet temperature extraction were investigated by means of different UDF's. The first method (UDF 1) required the temperature to be extracted from the control volumes immediately upstream of the heat-exchanger model. The second method (UDF 2) required the air temperature to be extracted immediately below the fan plane. A comparison between the results obtained by these two methods is shown in figure 4.2.

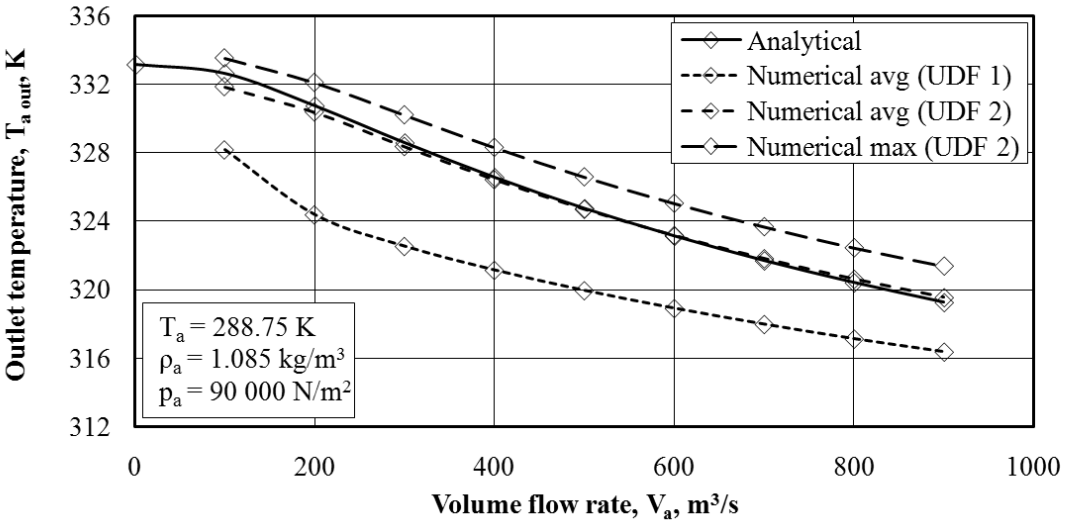

Figure 4.2: Comparison between analytically and numerically calculated fan-unit air outlet temperatures

Figure 4.2 shows a fairly large difference between the results obtained by the two temperature extraction methods. For the analytical solution, ambient temperature is taken as the air inlet temperature into the heat-exchanger. The same ambient temperature is therefore required as inlet condition to the numerical heat-exchanger model in order for these solutions to correlate. However, as figure 4.3 shows, significant numerical diffusion occurs between the volumes in and those immediately upstream of the heat-exchanger model, giving a faulty air inlet temperature to UDF 1, calculating the heat-transfer.

To mitigate this problem, UDF 1 was reconfigured to UDF 2. The latter UDF extracts the air temperatures on the fan rotating plane, rendering a solution that compares relatively well with the analytical solution. The numerically calculated air outlet temperature given in figure 4.2, is the averaged value of all the face temperatures on the outlet plane of the numerical heat-exchanger model. Figure 4.2 shows that the numerically calculated air outlet temperature deviates slightly from the analytical solution for low air flow rates.

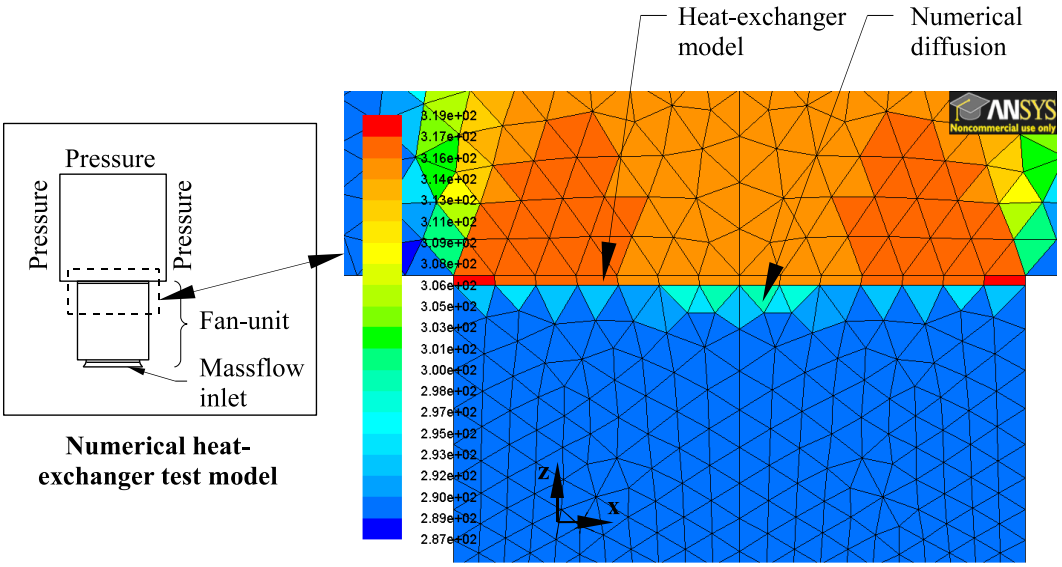

Figure 4.3: Temperature plot (K) showing numerical diffusion occurring between the heat-exchanger model and plenum chamber

The reason for deviation at low flow rates is, that the flow through some control volumes in the fan-unit model becomes essentially stagnant for low air flow rates, leading to very small heat source terms added to some volumes in the heat-exchanger model. Averaging the air temperature across the outlet face of the heat-exchanger model therefore renders a temperature value that is not entirely accurate, since only a fraction of the outlet plane has flow occurring through it. The maximum air temperature on the outlet plane of the heat-exchanger model also shows how the remaining active volumes (volumes that do have flow occurring through them) are approaching the analytical solution. The amount of energy transferred to the atmosphere is therefore still consistant with the analytical solution. Apart from this, a small number of fan units in the entire ACSC (0 - 7 %) work under these conditions and therefore the error made, if any, becomes insignificant. Consequently the latter heat-transfer model (UDF 2) was used for the remainder of the present study.

4.2 Comparison to previous work

The analysis of the Van Rooyen (2007) ACSC preceded the modeling of the large ACSC, in order to gain understanding and experience in the numerical modeling procedures involved and to verify the result obtained by Van Rooyen (2007). Similar verification was also done by Owen (2010) and Joubert (2010).

The Van Rooyen (2007) ACSC was subjected to a positive x-direction wind profile in the present study with a platform height magnitude of 3, 6 and 9 m/s

respectively. Figure 4.4 gives a comparison of the present results obtained for the volumetric effectiveness of certain fans in the Van Rooyen (2007) ACSC, to the previous results obtained by Van Rooyen (2007), Owen (2010) and Joubert (2010).

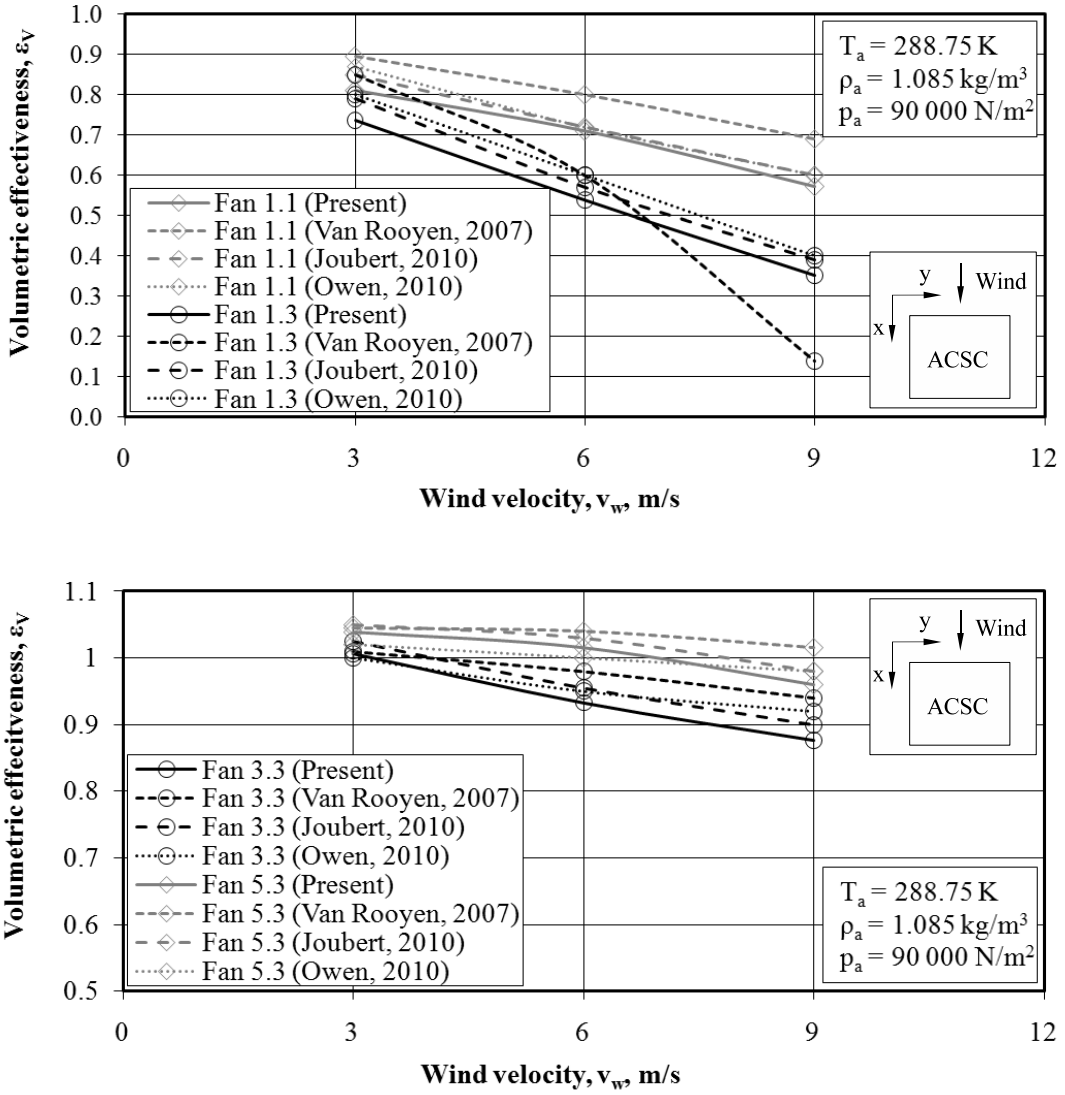

Figure 4.4: Comparison between the numerically predicted volumetric effectiveness of certain fans in the Van Rooyen (2007) ACSC under positive x-direction wind conditions

The results shown in figure 4.4, generally show fair correlation. It can be seen that fans on the leading edge of the ACSC are the fans severely affected by flow distortion. This is due to separation occurring along this edge, causing a decrease in static pressure beneath edge fans as well as distorted inflow

conditions. The fans further downstream are not as severely affected and even have the ability to exploit the energy in the wind, since the effectiveness is higher than 1 for certain fans.

The discrepancy between the present results and those obtained by Van Rooyen (2007), Owen (2010) and Joubert (2010) could be due to a number of reasons:

Firstly, the *actuator-disk* fan model was used by Van Rooyen (2007), whereas the *pressure-jump* method was used for fan modeling in the present study as well as the studies conducted by Owen (2010) and Joubert (2010). Both these models give an inaccurate prediction the fan performance under highly distorted inflow conditions (Van der Spuy *et al.*, 2009) and therefore some differences occur in the results obtained, especially for the edge fans. Secondly, the modeling procedure used in the present study is similar to Joubert (2010), but different from the studies of Van Rooyen (2007) and Owen (2010). Thirdly, a tetrahedral grid was used in the present study, whereas a structured hexahedral grid was used by Van Rooyen (2007) and unstructured hexahedral grids by Owen (2010) and Joubert (2010). The results obtained using different shapes of control volumes differ due control volume skewness and density.

Despite the discrepancies in volume flow rates through individual fans, the overall ACSC performance compares very well with that obtained by Van Rooyen (2007), Owen (2010) and Joubert (2010). A comparison between the various performances calculated for the Van Rooyen (2007) ACSC under a positive x-direction wind condition can be seen in figure 4.5.

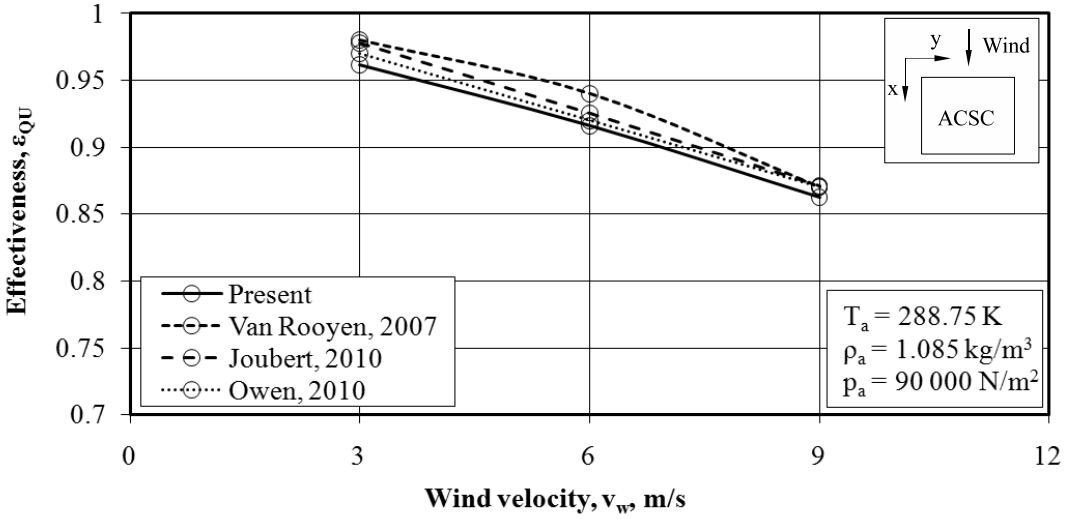

Figure 4.5: Comparison between the numerically predicted heat-transfer effectiveness of the Van Rooyen (2007) ACSC under positive x-direction wind conditions

4.3 Sensitivity analysis

A sensitivity analysis of the computational domain used in the *Iterative* modeling procedure was done to investigate the effect of boundary proximity to the ACSC model and to verify the computational accuracy of the grid. For this purpose three cases were individually investigated for a 3, 6 and 9 m/s positive x-direction wind and will be discussed hereafter.

Case 1 is referred to as the original case and is the analysis of the positive x-direction wind grid discussed in section 3.3.

Case 2 is similar to the original case with the distinction of a larger (dimensional) computational domain, but the grid size in the vicinity of the ACSC model remained the same as discussed in subsection 4.3.1.

Case 3 is similar to the original case in that the computational domain remained the same size (dimensional), but the grid is refined in the vicinity of the ACSC model as discussed in subsection 4.3.2 hereafter.

4.3.1 Boundary proximity

The ACSC is placed in an atmospheric environment, which is infinitely large compared to the ACSC. This poses the question of what the sufficient size (volumetric) of the computational domain should be in order to simulate the atmosphere.

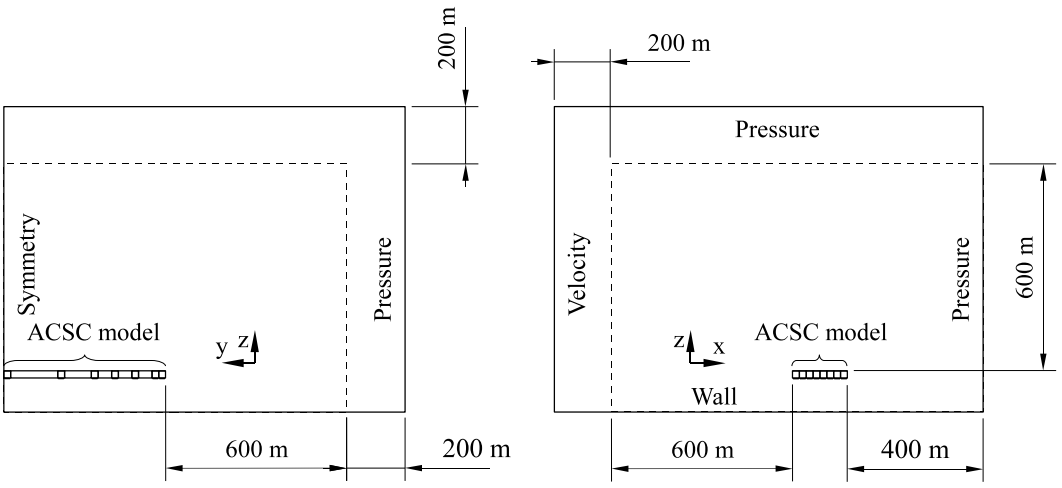

Figure 4.6: Dimensional adjustment to the positive x-direction wind computational domain

The boundary proximity of the computational domain were adjusted as shown in figure 4.6 to investigate the effect of a larger domain. After the analysis of the larger domain, the heat-transfer effectiveness was calculated for units 1, 2 and 3 and compared to the original case as shown in figure 4.7. Generally, good correlation can be seen, however some deviation of the original results occur for unit 1 and a 3 m/s wind. This error is still within five percent of the original value. It is therefore assumed that the dimensions of the original (case 1) computational domain is adequate since this error is marginal for the purpose of a trend analysis.

4.3.2 Grid density

The control volumes in the entire domain were refined especially in the vicinity of the ACSC, since it is expected that the most distorted flow will occur in this region and therefore a good grid density is important. The original and adjusted cell count is given in table 4.2.

Table 4.2: Cell count of the original and adjusted computational grid

Computational domain	Cell count
Large ACSC (original)	$8.25(10)^6$
Large ACSC (refined)	$11.87(10)^6$

Once again, a comparison of the heat-transfer effectiveness for units 1, 2 and 3 at the mentioned wind speeds is illustrated in figure 4.7. Good correlation between cases 1 and 3 is seen for all ACSC units, proving that the grid density of the original (case 1) computational domain is adequate for the present numerical analysis.

4.4 Convergence

Two measures of convergence were monitored in the present study, namely the convergence of flow through individual fans in a single simulation as well the convergence of flow in subsequent repititions of the *Iterative* procedure. These measures of convergence are discussed.

4.4.1 Convergence of a single simulation

For convenience the numbering used for fans in the Large ACSC is repeated as seen in figure 4.8:

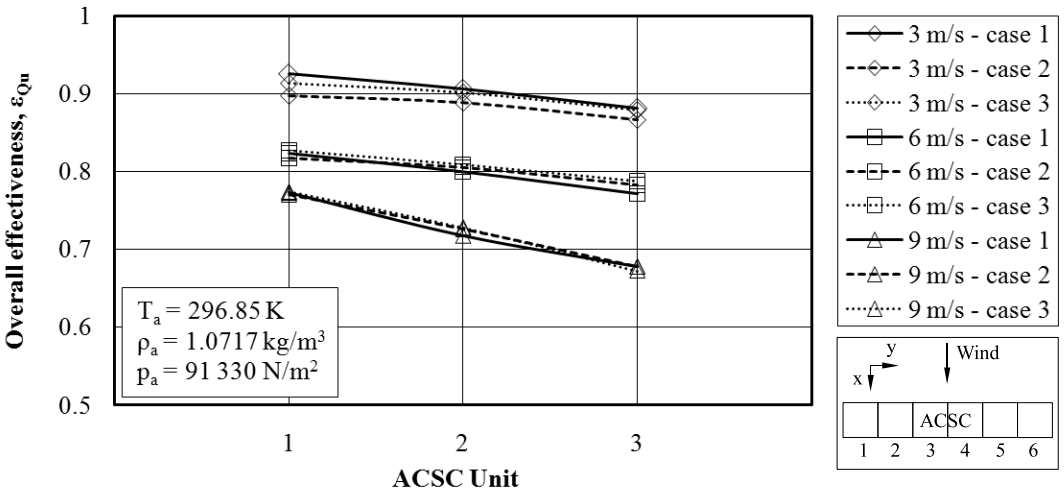

Figure 4.7: Comparison of the ACSC overall effectiveness for different wind speeds and computational grids

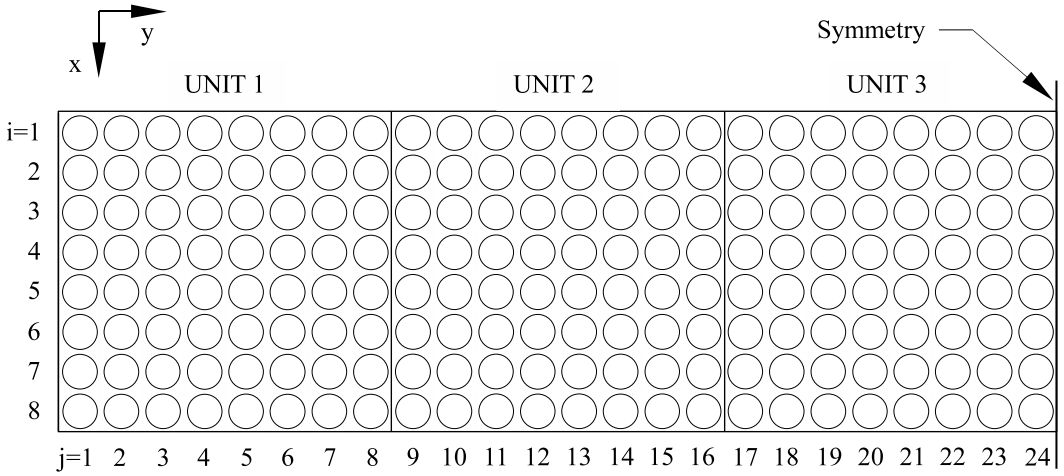

Figure 4.8: Numbering of individual fans used for the Large ACSC

Computational accuracy is also obtained by allowing the numerical solution to converge to an acceptable discrepancy. As mentioned in section 3.3, the convergence criterion in the present study was taken as $|V_{Fprevious} - V_{Fcurrent}| < 0.1$ m^3/s for individual fans.

The convergence of volume flow rate through certain fans in the first row of the ACSC, for a 6 m/s positive x-direction wind, is plotted in figure 4.9. It should be noted that the flow through fans receiving three-dimensional flow converge relatively fast compared to the fans in the two-dimensional flow region. Faster convergence of the solution was also obtained when skirts to the periphery of and screens below the ACSC were implemented.

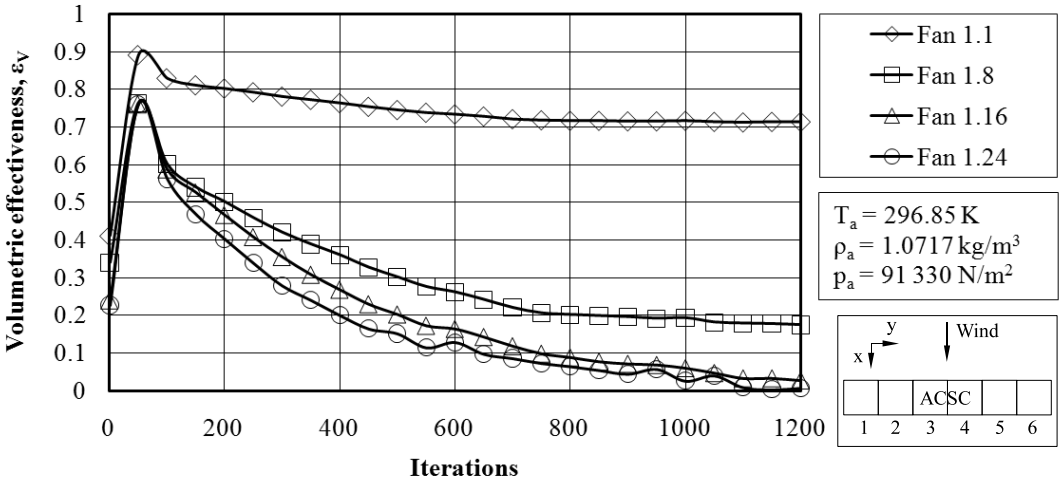

Figure 4.9: Convergence of volumetric flow rate through certain fans in row one of the Large ACSC

The poor convergence in the two-dimensional region is explained by the large amount of separation on the upstream edge of the ACSC, but will be discussed to more detail in chapter 5.

4.4.2 Convergence of subsequent simulations

Figure 4.10 shows the convergence of fan performance in the first row of the Large ACSC, subject to a positive x-direction wind of 6 m/s. It shows a relatively stable convergence of the volume flow through the fans and convergence is obtained after two repetitions of the *Iterative* method.

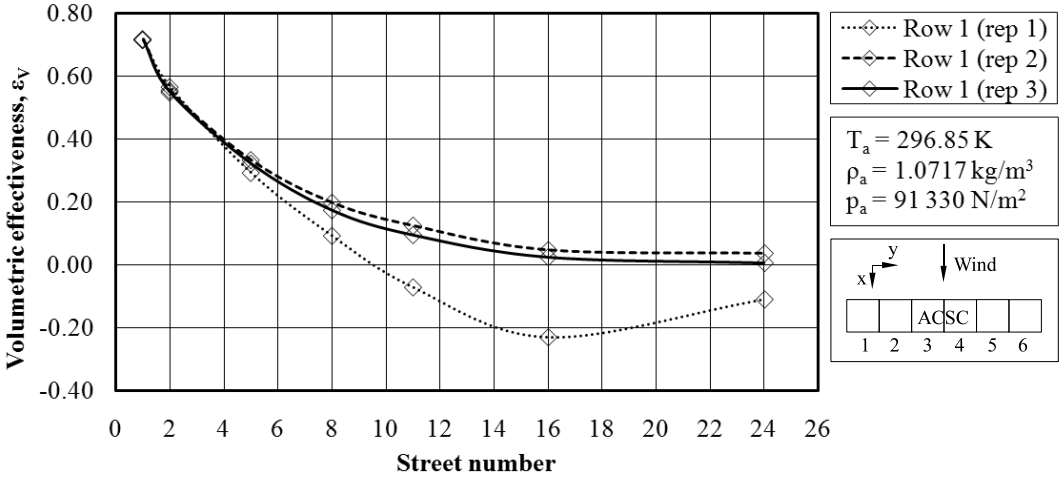

Figure 4.10: Convergence of row 1 in the Large ACSC subject to a 6 m/s positive x-direction wind obtained by the *Iterative* method